NASA
Technical Memorandum 4134

AVSCOM
Technical Report 89-B-004

# Measurement Resolution of Noise Directivity Patterns From Acoustic Flight Tests

David A. Conner

OCTOBER 1989

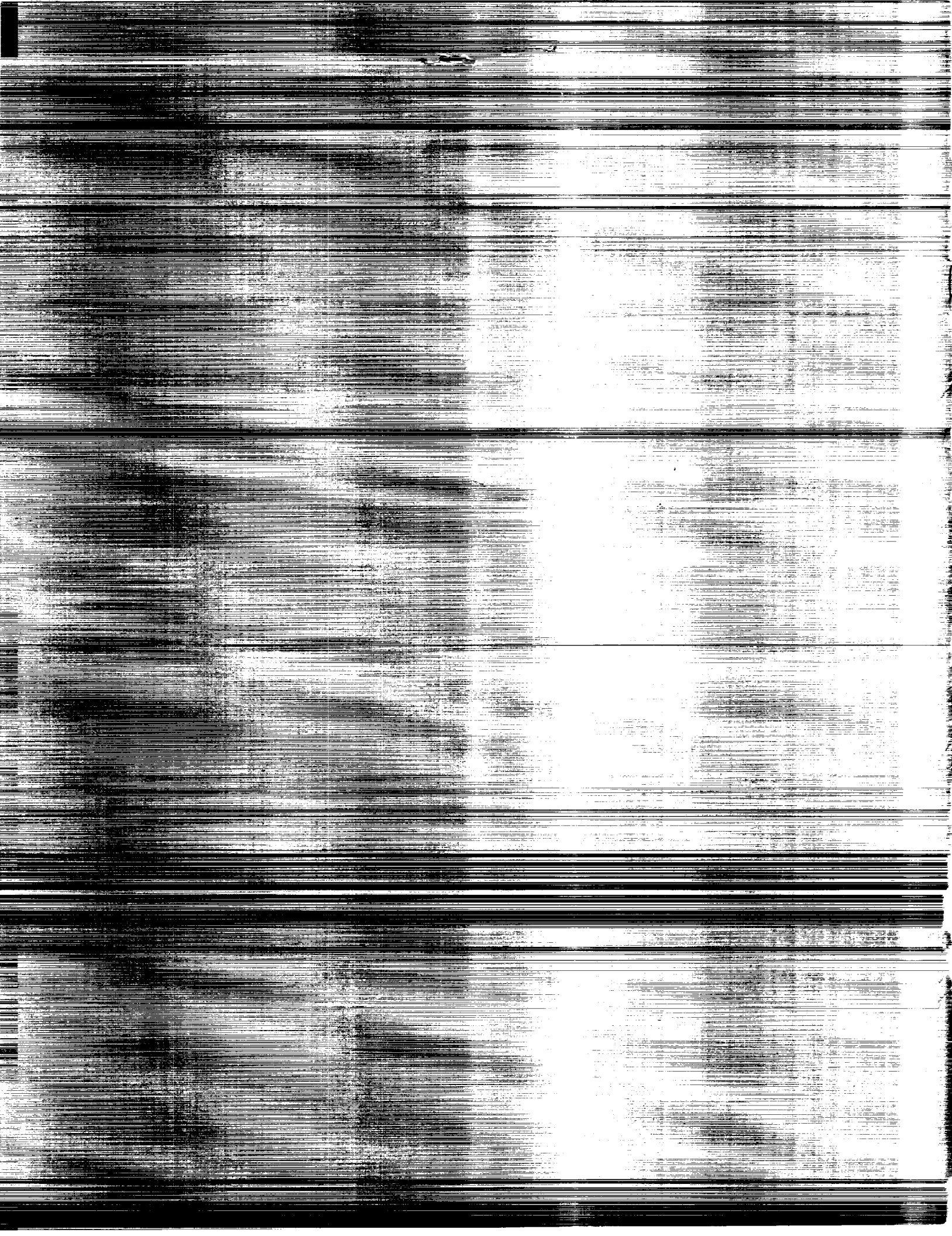

NASA
Technical Memorandum 4134

AVSCOM
Technical Report 89-B-004

# Measurement Resolution of Noise Directivity Patterns From Acoustic Flight Tests

David A. Conner
*Aerostructures Directorate*
*USAARTA-AVSCOM*
*Langley Research Center*
*Hampton, Virginia*

National Aeronautics and
Space Administration
Office of Management
Scientific and Technical
Information Division

**1989**

## Summary

A study was conducted to investigate the measurement resolution of noise directivity patterns from acoustic flight tests. Directivity-angle resolution is affected by the data reduction parameters, the aircraft velocity and flyover altitude, and deviations of the aircraft from the desired flight path. Equations are developed that determine bounds for the lateral- and longitudinal-directivity-angle resolution as a function of the nominal directivity angle. The equations are applied to a flight test data base, and the effects of several flight conditions and data reduction parameters on the directivity-angle resolution are presented. The maximum directivity-angle resolution typically occurs when the aircraft is at or near the overhead position. In general, directivity-angle resolution improves with decreasing velocity, increasing altitude, increasing sampling rate, decreasing block size, and decreasing block averages. Deviations from the desired ideal flight path will increase the resolution. For the flight experiment considered in this study, an average of two flyovers were required at each test condition to obtain an acceptable flight path. The ability of the pilot to maintain the flight path improved with decreasing altitude, decreasing velocity, and practice. Because of the prevailing wind conditions, yaw angles of as much as 20° were required to maintain the desired flight path.

## Introduction

In recent years helicopter noise has become a topic of great interest both within the helicopter community and to the public in general. This interest is precipitated, in part, by the increased noise levels of the modern helicopter due to increases in main rotor tip speed (ref. 1), flight speed, gross weight (ref. 1), and tail rotor tip speed (ref. 2). Compounding the problem of increased noise levels is a dramatic increase in the number of helicopters in use and a corresponding increase in demand for public-use heliports (ref. 3). Helicopter noise is different from most other types of aircraft noise in that it is periodic and impulsive. Powell and McCurdy (ref. 4) found that human annoyance to helicopter noise increased with the repetition rate of the periodic components and with impulsiveness by more than the equivalent of 4 dB and 13 dB, respectively. For these reasons, implementation of helicopter noise regulations is inevitable. Civilian noise limits are established for psychoacoustic criteria whereas military helicopters must be designed for minimum detectability since the military value of the helicopter for tactical and surveillance missions is reduced by its high-level and unique noise signature. The success of a new helicopter type could be seriously compromised by a design policy that does not consider noise.

A key element of a design for noise technology is an accurate rotorcraft noise-prediction methodology. ROTONET, a comprehensive computer prediction program currently under development at the Langley Research Center, predicts helicopter far-field noise levels and frequencies as a function of directivity angle (ref. 5). ROTONET accounts for spherical spreading (ref. 6), Doppler frequency shift (ref. 7), and atmospheric absorption (ref. 7) when propagating the source noise predictions to the far-field. Before this noise-prediction methodology will be generally accepted, however, it must be evaluated and proven with respect to the source noise elements incorporated.

One key element of the Langley work is the acquisition of a comprehensive, accurate, experimental acoustic data base to validate the predictions. This data base includes high-confidence, ground-level acoustic flyover data consisting of acoustic spectra as a function of the directivity angle, simultaneously measured helicopter dynamic state and spatial position data, and atmospheric data. To obtain the high-confidence levels required of the acoustic spectral estimates, an ensemble-averaging technique is employed in combination with a block-averaging technique which assumes that the signal is a stationary process over a short time period (ref. 8). Not considered by the technique, however, is the directivity-angle resolution of the averaged acoustic signal.

The purpose of this paper is to investigate the effects of various flight and analysis parameters on the directivity-angle resolution of the averaged acoustic spectra from an acoustic flyover test. In addition, some typical flight path and aircraft attitude data are presented from an acoustic flyover test conducted by NASA and the McDonnell Douglas Helicopter Company (MDHC) on a 500E helicopter at the NASA Wallops Flight Facility (WFF).

## Symbols

| | |
|---|---|
| $b$ | number of data points per block |
| $D$ | distance between adjacent microphones, ft |
| $N_B$ | number of blocks of data |
| $N_R$ | main rotor speed, rpm |
| $N_1$ | engine compressor speed, rpm |
| $N_2$ | engine output shaft speed (6016 rpm at 103-percent power), rpm |

| | |
|---|---|
| $n$ | microphone number |
| $T$ | analysis record length, sec |
| $T_B$ | length of data block, sec |
| $t_n$ | analysis start time for $n$th microphone, sec |
| $V$ | airspeed, knots |
| $v$ | aircraft velocity, ft/sec |
| $x, y, z$ | Cartesian coordinate system with origin at microphone 1 (reference microphone) |
| $\Delta Y$ | sideline deviation limits, ft |
| $Z$ | altitude, ft |
| $\Delta Z$ | altitude deviation limits, ft |
| $\alpha$ | angle of attack, deg |
| $\beta$ | angle of sideslip, deg |
| $\theta$ | longitudinal-directivity angle, deg |
| $\theta_{\text{crit1}}$ | first critical longitudinal-directivity angle, deg |
| $\theta_{\text{crit2}}$ | second critical longitudinal-directivity angle, deg |
| $\Delta\theta$ | longitudinal-directivity-angle resolution, deg |
| $\Delta\theta_{\text{meas}}$ | measured longitudinal-directivity-angle resolution, deg |
| $\Delta\theta_T$ | longitudinal-directivity-angle resolution due to block averaging, deg |
| $\Delta\theta_{TA}$ | longitudinal-directivity-angle resolution due to combined effects of block averaging and altitude deviation limits, deg |
| $\Delta\phi$ | lateral-directivity-angle resolution due to sideline deviation limits, deg |
| $\Delta\phi_{\text{meas}}$ | measured lateral-directivity-angle resolution, deg |
| $\Omega$ | rotor rotational speed, rpm |

Abbreviations:

| | |
|---|---|
| A/D | analog-to-digital |
| CH - WB | channel wideband |
| FFT | fast Fourier transform |
| HIARS | Helicopter Instrumentation and Recording System |
| MDHC | McDonnell Douglas Helicopter Company |
| MR | main rotor |
| mic | microphone |
| OASPL | overall sound pressure level, dB (re 0.0002 dynes/cm$^2$) |
| PCM | pulse code modulation |
| SPL | sound pressure level, dB (re 0.0002 dynes/cm$^2$) |
| SR | data sampling rate, samples per second |
| TOT | turbine output temperature, °C |
| TR | tail rotor |
| WFF | Wallops Flight Facility |

## Description of Experiment

### Test Helicopter

An acoustic flyover test was conducted at the NASA Wallops Flight Facility during a 4-week period in May and June 1986. The test aircraft was a modified McDonnell Douglas 500E experimental helicopter (fig. 1). The 500E helicopter has a 26.41-ft-diameter, fully articulated, five-bladed main rotor system with a 4.58-ft-diameter, two-bladed tail rotor; and it operates at a maximum gross weight of 3000 lb. In addition to the basic 500E helicopter hardware, an onboard research instrumentation system (described subsequently) and a four-bladed tail rotor and muffler were installed during parts of the flight test program.

### Onboard Instrumentation System

The onboard instrumentation system, referred to as the Helicopter Instrumentation and Recording System (HIARS), measures 31 different aircraft parameters, as indicated in table I, at data rates up to 5555 samples per second. The HIARS provides a modular, integrated, digital data acquisition system that can be installed onboard any passenger-carrying helicopter. A simplified system schematic is presented in figure 2, and a detailed description of the HIARS electronics system is provided in reference 9. The HIARS consists of a fuselage data acquisition and recording system that fits in the rear seat/cargo area of the helicopter, a rotor-mounted data acquisition and telemetry system, and a 1/rev and 256/rev signal ring with integrated telemetry transmitting antenna that mounts on the rotating swash plate.

The HIARS utilizes an advanced, rotor-mounted, 8-bit pulse code modulation (PCM) telemetry system to acquire main rotor measurements and a second 10-bit PCM system to acquire fuselage performance measurements. The fuselage data system receives the rotor telemetry signal, merges the rotor and fuselage PCM signals in a master-slave configuration, and provides magnetic tape storage of all data from both systems. The fuselage system incorporates a modern commercial PCM subsystem to multiplex the various analog and digital transducer signals into a serial digital format for onboard recording. A 14-track, direct-recording magnetic tape recorder with wideband II response was operated at 30 in/sec to record all aircraft data.

Helicopter pitch and yaw attitudes were measured using standard flight-certified gyroscopic sensors. Pitch angle measurements were obtained using a standard displacement gyroscope, whereas yaw angle or heading measurements were obtained using a north-slaved gyroscope.

### Tracking Instrumentation System

The aircraft position tracking system consisted of a laser system in conjunction with a FPS-16 radar system. In the event that the laser lock is lost, the tracking system reverts to the FPS-16 radar system which tracks a C-band transponder mounted on the test vehicle. Real-time $xy$ and $xz$ plots provided immediate verification of the flight path acceptability. The tracking data were postprocessed by translating the coordinate system origin to the reference microphone position and rotating the coordinate system to align it with the desired flight path. The postprocessed tracking data, in the form of time histories in both the spherical and Cartesian coordinate systems, were recorded on magnetic tape at a rate of 10 points per second, along with time code. Tracking data are presented in Cartesian coordinates from the postprocessed data.

### Meteorological Instrumentation System

A small, tethered, blimp-shaped balloon was used to lift instrumentation that provided meteorological data before and during the flight tests (ref. 10). Profiles of temperature, relative humidity, and wind speed and direction were measured up to the maximum test altitude. The output of the package was telemetered to an instrument van on the ground, where it was displayed in real time and was recorded on magnetic tape. Additional weather information was obtained from a permanent weather station at the WFF. The permanent weather station had a sensor height of 10 m and measured wind speed and direction, barometric pressure, and dew point in the form of strip charts.

Weather forecasts from the permanent weather station were used to determine the acceptability of weather conditions for flight testing on the following day. Weather conditions that precluded flight testing were steady ground-level winds of 10 knots or greater, relative humidity in excess of 95 percent, or precipitation. Atmospheric weather profiles obtained from the weather balloon system were used to account for the propagation of the acoustic signal from the source to the receiver.

### Acoustic Instrumentation and Flight Test Procedures

The acoustic instrumentation consisted of 24 microphone systems operated from 2 mobile data vans. The microphones were positioned into four linear arrays of six microphones each as illustrated in figure 3. The distance between adjacent microphones within each array was 200 ft, whereas the distance between arrays was 250 ft. Each microphone was fitted with a grid cap and wind screen and was mounted on a 4- by 4-ft plywood ground board. Each microphone signal was amplified, band-pass filtered between 20 Hz and 16 kHz, and recorded (along with time code) on a frequency-modulated, 14-track wideband I tape recorder operating at 15 in/sec. A pistonphone was used in the field each day for sound level calibration.

A typical data run scenario begins approximately 2 miles out from the microphone array. The pilot aligns the aircraft with the desired flight path (see fig. 3) and attains the proper altitude and airspeed. Direct communications between the aircraft pilot and a radar technician are utilized to help maintain an acceptable flight track. The radar technician, viewing the $xy$ and $xz$ tracking data in real time, recommends flight path corrections when necessary to maintain the flight path within acceptable limits. At approximately 1 mile out all data systems are turned on. The aircraft, flying at constant altitude and airspeed, passes over the microphone array and continues on this course until it is approximately 1 mile past the array. At this point all data systems are turned off and the data run is complete. Immediately after completion of the data run, an assessment is made of the flight path acceptability and acoustic data quality to determine whether a repeat of the run is required.

## Data Reduction and Analysis

### Aircraft Flight Data Reduction

The HIARS data reduction process consisted of demultiplexing the original serial digital data stream back into the individual components and converting

each of these components to their respective engineering units. Pitch and yaw measurements were obtained at a rate of 231 samples per second, and the 256/rev measurements were obtained at a rate of 5555 samples per second.

### Acoustic Data Reduction

The acoustic source field produced by an aircraft moving at constant altitude, velocity, attitude, and engine power setting through a uniform atmosphere represents a stationary random process. The acoustic signal received from a moving aircraft at a fixed observer position, however, is nonstationary. In addition to the well-known Doppler effect, the characteristics of the spectrum of the received signal change because of the directionality of the source, spherical spreading, atmospheric absorption, and ground reflection and attenuation. Since the techniques of time series analysis are valid only for data that satisfy conditions of weak stationarity (refs. 11 and 12), the received acoustic signal is assumed to be weakly stationary over some sufficiently small time interval. However, small analysis time intervals result in few statistical degrees of freedom and poor confidence in the sound pressure level estimates. To circumvent this dilemma, a technique of ensemble-averaging spectra over several microphones is applied (ref. 8).

The procedure for reducing the experimental data is as follows. Directivity angles are calculated from aircraft position and estimated angle of attack. Reception times are calculated by assuming that the sound propagates in a straight line at a constant average speed determined from meteorological data obtained from the balloon system during testing. The average velocity of the aircraft during the flyover is also calculated. To analyze the data according to directivity angle, data records are interpolated to determine signal reception times corresponding to the emission angles of interest.

For the 500E test, the analog acoustic tapes were sampled at a rate of 25 000 samples per second and digitized with an amplitude resolution of 3600 counts full scale. In order to ensemble-average spectra from different microphones, the individual spectra must be calculated from data segments based on an identical aircraft-to-microphone directivity angle. With the microphones equally spaced along a line parallel to the flight path, it is necessary to shift the data for each microphone by a time $t_n$ defined as

$$t_n = (n-1)\frac{D}{v} \qquad (1)$$

where $n$ is the microphone number, $D$ is the distance between adjacent microphones, and $v$ is the aircraft velocity.

For each time corresponding to a directivity angle of interest, one segment of data centered on that time is found for each microphone. Each segment is separated into blocks, a Hanning data window is applied, and a spectrum is calculated for each block. The block spectra are then averaged to provide a block-averaged spectral estimate for each segment. The block-averaged spectra corresponding to each directivity angle of interest are then ensemble-averaged over all microphones. Each ensemble-averaged analysis consists of 5 blocks of 2048 points each per microphone for a frequency resolution of approximately 12 Hz and an 80-percent confidence interval of -1.08 to 0.90 dB about the estimate based on a chi-square distribution. The advantage of this ensemble-averaging technique is that it averages pressure spectra from "$N$" microphones from one aircraft flyover rather than the more typical method of averaging pressure spectra from "$N$" flyovers of one microphone. This technique greatly reduces the required flight time while assuring very similar flight conditions for all data used in the ensemble-averaging process.

## Resolution of Longitudinal and Lateral Directivity Angles

An important consideration in any acoustic flyover test is the directivity of the noise field radiated by the aircraft. For highly directional aircraft, such as helicopters, the resolution of the directivity angle of the acoustic measurement becomes most important. As an example, figures 4 and 5 present predicted horizontal and vertical noise directivity patterns for thickness noise and loading noise, respectively, for a typical four-bladed helicopter in forward flight (ref. 13). To define the horizontal directivity pattern due to thickness noise in terms of the overall sound pressure level (OASPL), figure 4(a) shows that a directivity-angle resolution of 15°, for example, is sufficient. However, at the longitudinal-directivity angle of approximately 110°, a directivity-angle resolution of 15° would alter the noise contours for the vertical directivity pattern due to thickness noise presented in figure 4(b). The horizontal directivity pattern due to loading noise presented in figure 5(a) indicates that a directivity-angle resolution of 15° is sufficient if the OASPL or the sound pressure level (SPL) of the first harmonic is of interest. However, a finer directivity-angle resolution would be required to avoid averaging out the lobular patterns of the SPL of the second and third harmonics. Figure 5(b) shows that a directivity-angle resolution of 15° is sufficient to represent the vertical directivity pattern of the OASPL due to loading noise for any

longitudinal-directivity angle. In general, the more lobular the pattern, the finer the directivity-angle resolution required to accurately reproduce the actual phenomena.

In designing a flight test plan for aircraft noise measurements, the directivity-angle resolution of the averaged acoustic spectra must be considered. Directivity-angle resolution is affected by the data reduction parameters, the aircraft velocity and altitude, and the deviations of the aircraft from the desired straight-and-level flight path. The following three subsections will discuss the effects of the averaging technique and the effects of the vertical and horizontal flyover envelopes on the acoustic directivity-angle resolution. Plots of the directivity-angle resolution as a function of the nominal directivity angle are presented for a typical flyover. The flight conditions and data reduction parameters for these plots are given in table II. Finally, the effect of different parameters on the directivity-angle resolution will be discussed.

### Effect of Block Averaging

The time interval or record length ($T$) required to obtain the necessary data for the block-averaging analysis is defined as

$$T = N_B \times T_B \tag{2}$$

where $N_B$ is the number of blocks of data and $T_B$ is the length of data block.

During this time interval the aircraft travels a given distance. The change in the longitudinal-directivity angle due to the aircraft travel defines the longitudinal-directivity-angle resolution due to block averaging ($\Delta\theta_T$) as illustrated in figure 6(a). The equation for $\Delta\theta_T$ as a function of the longitudinal-directivity angle ($\theta$) is

$$\Delta\theta_T = \tan^{-1}\left(\frac{Z}{Z/\tan\theta - vT/2}\right) - \tan^{-1}\left(\frac{Z}{Z/\tan\theta + vT/2}\right) \tag{3}$$

where $\theta$ is the longitudinal-directivity angle, $Z$ is the altitude, $v$ is the aircraft velocity, and $T$ is the record length (see eq. (2)). Figure 6(b) presents a plot of the variation of $\Delta\theta_T$ as a function of $\theta$ for a typical flight condition. In the overhead position (where $\theta = 90°$), $\Delta\theta_T$ has a maximum of nearly 13°. The shape of this curve is typical for any chosen parameters, and only the magnitude of $\Delta\theta_T$ varies with these parameters.

### Effect of Altitude Variations

Variations in the aircraft altitude during a flyover will increase the longitudinal-directivity-angle resolution. Consider the aircraft as it approaches the microphone array as shown in figure 7(a). The data reduction parameters along with the aircraft velocity and the altitude deviation limits provide a "data box" that is $V \times T$ ft long by 2 $\Delta Z$ ft high, where $\Delta Z$ is the altitude deviation limit. The analysis averages the acoustic signal measured while the aircraft moves through this data box. When approaching the microphone array the maximum longitudinal-directivity-angle resolution due to the combined effects of block averaging and altitude deviation limits ($\Delta\theta_{TA}$) would be obtained if the aircraft entered the data box from the lower right-hand corner and exited through the upper left-hand corner. As the aircraft nears the overhead position where $\theta$ is greater than some critical longitudinal-directivity angle ($\theta_{\text{crit1}}$) and less than a second critical longitudinal-directivity angle ($\theta_{\text{crit2}}$), the maximum $\Delta\theta_{TA}$ would be obtained if the aircraft passed through the entire data box while at the lower altitude limit. The equations for these critical directivity angles are

$$\theta_{\text{crit1}} = \tan^{-1}(2Z/vT) \tag{4}$$

$$\theta_{\text{crit2}} = 90° + (90 - \theta_{\text{crit1}}) \tag{5}$$

For $\theta > \theta_{\text{crit2}}$, the maximum $\Delta\theta_{TA}$ would be obtained if the aircraft entered the data box from the upper right-hand corner and exited through the lower left-hand corner. This maximum resolution-angle scenario indicates that for an approaching aircraft, a sudden drop in altitude will produce less of an increase in $\Delta\theta_{TA}$ than would a sudden increase in altitude. Conversely, for a departing aircraft, a sudden increase in altitude is preferable to a sudden drop in altitude. In the near-overhead position, the greater the altitude the smaller the resultant angular resolution. The equations for maximum $\Delta\theta_{TA}$ as a function of $\theta$ are, for $0° < \theta \leq \theta_{\text{crit1}}$,

$$\Delta\theta_{TA} = \tan^{-1}\left(\frac{Z + \Delta Z}{Z/\tan\theta - vT/2}\right) - \tan^{-1}\left(\frac{Z - \Delta Z}{Z/\tan\theta + vT/2}\right) \tag{6}$$

for $\theta_{\text{crit1}} \leq \theta \leq \theta_{\text{crit2}}$,

$$\Delta\theta_{TA} = \tan^{-1}\left(\frac{Z - \Delta Z}{Z/\tan\theta - vT/2}\right) - \tan^{-1}\left(\frac{Z - \Delta Z}{Z/\tan\theta + vT/2}\right) \tag{7}$$

and, for $\theta_{crit2} \leq \theta < 180°$,

$$\Delta\theta_{TA} = \tan^{-1}\left(\frac{Z - \Delta Z}{Z/\tan\ \theta - vT/2}\right) - \tan^{-1}\left(\frac{Z + \Delta Z}{Z/\tan\ \theta + vT/2}\right) \quad (8)$$

Figure 7(b) presents a plot of the variation of $\Delta\theta_{TA}$ as a function of $\theta$ for a typical flight condition. The $\Delta\theta_{TA}$ curve is symmetric about $\theta = 90°$ with a maximum of 14° at $\theta = 72°$ and 108° and a decrease of about 0.5° near $\theta = 90°$. The shape of this curve is typical for any selected parameters; however, the location(s) and magnitude of the maximum resolution angle can vary significantly with flight and data reduction parameters.

### Effect of Sideline Variations

Variations in the aircraft sideline track will produce a sideline or lateral-directivity-angle resolution ($\Delta\phi$) as shown in figure 8(a). The data reduction parameters, aircraft velocity, and sideline deviation limits produce a data box that is $V \times T$ ft long by 2 $\Delta Y$ ft wide, where $\Delta Y$ is the sideline deviation limit. The analysis averages the acoustic signal measured while the aircraft moves through this data box. The maximum $\Delta\phi$ would be obtained if the aircraft were to traverse the data box instantaneously from one sideline limit to the opposite sideline limit at the point within the data box where the aircraft is closest to the microphone. The equations for $\Delta\phi$ as a function of $\theta$ are, for $0° < \theta \leq \theta_{crit1}$,

$$\Delta\phi = 2 \times \tan^{-1}\left\{\frac{\Delta Y}{\left[(Z/\tan\ \theta - vT/2)^2 + Z^2\right]^{1/2}}\right\} \quad (9)$$

for $\theta_{crit1} \leq \theta \leq \theta_{crit2}$,

$$\Delta\phi = 2 \times \tan^{-1}\left(\frac{\Delta Y}{Z}\right) \quad (10)$$

and, for $\theta_{crit2} \leq \theta < 180°$,

$$\Delta\phi = 2 \times \tan^{-1}\left\{\frac{\Delta Y}{\left[(Z/\tan\ \theta + vT/2)^2 + Z^2\right]^{1/2}}\right\} \quad (11)$$

Figure 8(b) presents a plot of the variation of $\Delta\phi$ as a function of $\theta$ for a typical flight condition. The $\Delta\phi$ curve is symmetric about $\theta = 90°$ with a maximum of 9° in the overhead position between $\theta_{crit1}$ and $\theta_{crit2}$. The maximum $\Delta\phi$ is most critical when $\theta_{crit1} \leq \theta \leq \theta_{crit2}$.

### The Combined Effects of Block Averaging, Altitude Variations, and Sideline Variations

The previous paragraphs have introduced the concepts of directivity-angle resolution due to three different parameters: the time period required for data acquisition, the altitude, and the sideline deviation limits. To consider the combined effects of analysis time, altitude variations, and sideline variations, the data box becomes three-dimensional ($V \times T$ ft long by 2 $\Delta Y$ ft wide by 2 $\Delta Z$ ft high). Because the analysis fixes the time period required for data acquisition and assumes that the test aircraft does not deviate from the desired flight path, $\Delta\theta_T$ is the minimum longitudinal-directivity-angle resolution available. Sideline deviations have no effect on the longitudinal angular resolution; therefore, $\Delta\theta_{TA}$ is the maximum longitudinal-directivity-angle resolution. Figure 9 combines $\Delta\theta_T$ and $\Delta\theta_{TA}$ versus $\theta$ for a typical flight condition. The solid curve is $\Delta\theta_T$ and represents the minimum directivity-angle resolution available for all angles of $\theta$. The maximum directivity-angle resolution ($\Delta\theta_{TA}$) is plotted as a dashed line. The longitudinal-directivity-angle resolution of the measured acoustic signal ($\Delta\theta_{meas}$) for any $\theta$ will fall somewhere between the curves of $\Delta\theta_T$ and $\Delta\theta_{TA}$, depending on the manner and the magnitude of the aircraft deviations from the desired test altitude as the aircraft passes through the data box (i.e., $\Delta\theta_T \leq \Delta\theta_{meas} \leq \Delta\theta_{TA}$). For example, at $\theta = 60°$, $10° \leq \Delta\theta_{meas} \leq 13°$.

Although the sideline deviation limits have no effect on the longitudinal-directivity-angle resolution, the altitude deviation limits do affect the lateral-directivity-angle resolution. If the aircraft were to pass through the three-dimensional data box at the lower altitude limit, the distance $d_2$ in figure 8(a) would decrease slightly; and since $\Delta Y$ is held constant, $\Delta\phi$ would increase. However, because this increase in $\Delta\phi$ is very small, the effect of altitude deviations on $\Delta\phi$ is not considered in this paper. Figure 8(b), then, presents the maximum lateral-directivity-angle resolution considered in this paper. The lateral-directivity-angle resolution of the measured acoustic signal ($\Delta\phi_{meas}$) for any $\theta$ will fall somewhere between 0° and the curve of $\Delta\phi$, again depending on the manner and the magnitude of the aircraft deviations from the ideal flight path as the aircraft passes through the data box (i.e., $0° \leq \Delta\phi_{meas} \leq \Delta\phi$). For the flight conditions listed in table III, at $\theta = 60°$, it is found that $0° \leq \Delta\phi_{meas} \leq 8°$.

## Calculations of Directivity-Angle Resolution for Various Parameters

### Angle Resolution for Range of Velocities

Figure 10 presents plots of the longitudinal-directivity-angle resolution boundaries versus the nominal directivity angle for aircraft velocities of 40 to 140 knots in 20-knot increments. The maximum $\Delta\theta_{TA}$ occurs in the overhead position ($\theta = 90°$) at the higher velocities and moves progressively farther away from the overhead position as the velocity decreases while always maintaining symmetry about $\theta = 90°$. The maximum $\Delta\theta_{TA}$ decreases from nearly 24° at 140 knots to approximately 9° at 40 knots while the location moves from $\theta = 90°$ for velocities of 100 knots or greater to approximately 28° away from the overhead position at 40 knots. The maximum $\Delta\theta_T$ always occurs at $\theta = 90°$ and decreases from 22° at 140 knots to approximately 6° at 40 knots.

The maximum $\Delta\phi$ is independent of velocity; however, the values of the critical longitudinal-directivity angles ($\theta_{crit1}$ and $\theta_{crit2}$) are not. Figure 11 presents a plot of $\Delta\phi$ versus $\theta$ for velocities of 40 and 140 knots. For both velocities presented, the maximum $\Delta\phi$ is approximately 9° and occurs for $\theta_{crit1} \leq \theta \leq \theta_{crit2}$. For $0° < \theta < \theta_{crit1}$, the 140-knot curve is slightly greater than the 40-knot curve, and this difference generally increases with increasing $\theta$. As $\theta$ increases from $\theta_{crit2}$ toward 180°, the 140-knot curve is again greater but the difference generally decreases with increasing $\theta$. Increasing velocity decreases the value of $\theta_{crit1}$ and increases the value of $\theta_{crit2}$, thereby increasing the width of the region of maximum $\Delta\phi$. At 40 knots, this region is $87° \leq \theta \leq 93°$ and increases to $79° \leq \theta \leq 101°$ at 140 knots.

From figures 10 and 11 it can be concluded that the directivity-angle resolution, both lateral and longitudinal, is the smallest at low velocities and increases with increasing velocity.

### Angle Resolution for Range of Altitudes

Figure 12 presents plots of the longitudinal-directivity-angle resolution boundaries versus the nominal directivity angle for test altitudes of 100, 250, 500, and 750 ft. The maximum $\Delta\theta_{TA}$ occurs at $\theta = 90°$ for the 100-ft-altitude case and moves progressively farther away from the overhead position with increasing altitude while always maintaining symmetry about $\theta = 90°$. The maximum $\Delta\theta_{TA}$ decreases from approximately 38° at a 100-ft altitude to approximately 5° at a 750-ft altitude, whereas the location moves from $\theta = 90°$ at a 100-ft altitude to approximately 18° away from the overhead position at a 750-ft altitude. The maximum $\Delta\theta_T$ always occurs at $\theta = 90°$ and decreases from 31° at a 100-ft altitude to approximately 4° at a 750-ft altitude.

Figure 13 presents a plot of $\Delta\phi$ versus $\theta$ for altitudes of 100, 250, 500, and 750 ft. The maximum $\Delta\phi$ decreases from nearly 23° at a 100-ft altitude to approximately 3° at a 750-ft altitude, and this maximum angle occurs for $\theta_{crit1} \leq \theta \leq \theta_{crit2}$. In addition, decreasing altitude decreases the value of $\theta_{crit1}$ and increases the value of $\theta_{crit2}$, thereby increasing the width of the region of maximum $\Delta\phi$. At a 100-ft altitude, this region is $75° \leq \theta \leq 105°$ and decreases to $88° \leq \theta \leq 92°$ at a 750-ft altitude.

From figures 12 and 13 it can be concluded that both the lateral- and longitudinal-directivity-angle resolutions are smallest at high altitude.

### Angle Resolution for Range of Sampling Rates

Figure 14 presents plots of the longitudinal-directivity-angle resolution boundaries versus the nominal directivity angle for sampling rates (SR) of 15 000 (15K) to 40 000 (40K) samples per second. The maximum $\Delta\theta_{TA}$ occurs in the overhead position for the 15K and 20K SR cases and moves progressively farther away from the overhead position with increasing SR while always maintaining symmetry about $\theta = 90°$. The maximum $\Delta\theta_{TA}$ decreases from nearly 23° for a 15K SR to 10° for a 40K SR, whereas the location moves from $\theta = 90°$ for the two lowest sampling rates to approximately 23° away from the overhead position for the highest SR. The maximum $\Delta\theta_T$ always occurs at $\theta = 90°$ and decreases from approximately 21° for the 15K SR case to just less than 8° for the 40K SR case.

The maximum $\Delta\phi$ is not affected by sampling rate; however, the values of the critical longitudinal-directivity angles ($\theta_{crit1}$ and $\theta_{crit2}$) are affected. Figure 15 presents a plot of the lateral-directivity-angle resolution versus the nominal directivity angle for sampling rates of 15K and 40K samples per second. For both sampling rates presented, the maximum $\Delta\phi$ is 9° and occurs for $\theta_{crit1} \leq \theta \leq \theta_{crit2}$. For $0° < \theta < \theta_{crit1}$, the 15K sampling rate curve is slightly greater than the 40K sampling rate curve, and this difference generally increases with increasing $\theta$. As $\theta$ increases from $\theta_{crit2}$ toward 180°, the 15K curve is again greater but the difference generally decreases with increasing $\theta$. Increasing the sampling rate increases the value of $\theta_{crit1}$ and decreases the value of $\theta_{crit2}$, thereby decreasing the width of the region of maximum $\Delta\phi$. For the 15K sampling rate, this region is $80° \leq \theta \leq 100°$ and decreases to $86° \leq \theta \leq 94°$ for the sampling rate of 40K samples per second.

From figures 14 and 15 it can be concluded that the lateral- and longitudinal-directivity-angle resolutions are smallest at high sampling rates. Increasing the sampling rate not only increases the data file size but also increases the maximum frequency of the spectra.

### Angle Resolution for Range of Block Size

Figure 16 presents plots of the longitudinal-directivity-angle resolution boundaries versus the nominal directivity angle for block sizes of 512, 1024, 2048, and 4096 samples. The maximum $\Delta\theta_{TA}$ occurs at $\theta = 90°$ for the largest block size and moves progressively farther away from the overhead position as the block size decreases while always maintaining symmetry about $\theta = 90°$. The maximum $\Delta\theta_{TA}$ decreases from 27° for $b = 4096$ to approximately 6° for $b = 512$ while the location moves from $\theta = 90°$ for the largest block size to approximately 36° away from the overhead position for the smallest block size. The maximum $\Delta\theta_T$ always occurs at $\theta = 90°$ and decreases from 25° for $b = 4096$ to approximately 3° for $b = 512$.

The maximum $\Delta\phi$ is not affected by block size; however, the values of the critical longitudinal-directivity angles ($\theta_{\text{crit1}}$ and $\theta_{\text{crit2}}$) are affected. Figure 17 presents a plot of $\Delta\phi$ versus $\theta$ for block sizes of 512 and 4096. For both block sizes presented, the maximum $\Delta\phi$ is approximately 9° and occurs for $\theta_{\text{crit1}} \leq \theta \leq \theta_{\text{crit2}}$. For $0° < \theta < \theta_{\text{crit1}}$, the 4096 block size curve is slightly greater than the 512 block size curve, and this difference generally increases with increasing $\theta$. As $\theta$ increases from $\theta_{\text{crit2}}$ toward 180°, the 4096 block size curve is again greater but the difference generally decreases with increasing $\theta$. Increasing the FFT block size decreases the value of $\theta_{\text{crit1}}$ and increases the value of $\theta_{\text{crit2}}$, thereby increasing the width of the region of maximum $\Delta\phi$. For $b = 4096$, this region is $78° \leq \theta \leq 102°$ and decreases to $88° \leq \theta \leq 92°$ for $b = 512$.

From figures 16 and 17 it can be concluded that the lateral- and longitudinal-directivity-angle resolutions are minimized with decreasing block size. Decreasing the block size not only reduces the frequency resolution of the spectral analysis but also reduces the required computation time.

### Angle Resolution for Range of Block Averages

Figure 18 presents plots of the longitudinal-directivity-angle resolution boundaries versus the nominal directivity angle for the usage of 1, 3, 5, 7, and 9 block averages ($N_B$). The maximum $\Delta\theta_{TA}$ occurs at $\theta = 90°$ for the $N_B = 7$ and 9 cases and moves progressively farther away from the overhead position with decreasing $N_B$ while always maintaining symmetry about $\theta = 90°$. The maximum $\Delta\theta_{TA}$ decreases from nearly 25° for $N_B = 9$ to approximately 6° for $N_B = 1$, whereas the location moves from $\theta = 90°$ for $N_B = 7$ and 9 to approximately 38° away from the overhead position for $N_B = 1$. The maximum $\Delta\theta_T$ always occurs at $\theta = 90°$ and decreases from nearly 23° for $N_B = 9$ to approximately 2.5° for $N_B = 1$.

The maximum $\Delta\phi$ is not affected by the number of block averages; however, the values of the critical longitudinal-directivity angles ($\theta_{\text{crit1}}$ and $\theta_{\text{crit2}}$) are affected. Figure 19 presents a plot of $\Delta\phi$ versus $\theta$ for $N_B = 1$ and 9. For both $N_B = 1$ and 9, the maximum $\Delta\phi$ is approximately 9° and this maximum angle occurs for $\theta_{\text{crit1}} \leq \theta \leq \theta_{\text{crit2}}$. For $0° < \theta < \theta_{\text{crit1}}$, the $N_B = 9$ curve is slightly greater than the $N_B = 1$ curve, and this difference generally increases with increasing $\theta$. As $\theta$ increases from $\theta_{\text{crit2}}$ toward 180°, the $N_B = 9$ curve is again greater but the difference generally decreases with increasing $\theta$. Decreasing $N_B$ increases the value of $\theta_{\text{crit1}}$ and decreases the value of $\theta_{\text{crit2}}$, thereby decreasing the width of the region of maximum $\Delta\phi$. For the case of $N_B = 9$, this region is $79° \leq \theta \leq 101°$ and decreases to $89° \leq \theta \leq 91°$ for $N_B = 1$.

It can be concluded that the lateral- and longitudinal-directivity-angle resolutions are smallest with a small $N_B$. However, decreasing the number of block averages reduces the confidence interval of the sound pressure levels provided by the analysis.

## Assessment of 500E Flyover Experiment

### Variability of Aircraft Flight Path

As a result of recognizing that the aircraft cannot fly a perfectly straight-and-level flight path, limits on the flight path variations must be set. In the previous section it was shown that data reduction techniques can provide some adjustment to the directivity-angle resolution; however, deviations from the desired flight path strongly influence the resolution. For the 500E flight test program, the test matrix included a range of aircraft velocities, altitudes, gross weights, and main rotor rotational speeds ($N_2$). The vast majority of runs were conducted at 80 or 120 knots, 250- or 750-ft altitude, 3000-lb gross weight, and 103-percent $N_2$. Because it was not known how well this helicopter could maintain a flight path, limits were selected that would provide reasonable conditions for the analysis. At each of the test altitudes a "box" covering the sideline and altitude variations was selected. Table III lists the altitude and sideline deviation limits for each altitude, along with the magnitude and location of associated maximum

directivity-angle resolutions. In this section an evaluation of the vehicle to remain within this box for the various test conditions of velocity, altitude, vehicle gross weight, and main rotor rotational speed ($N_2$) will be presented.

Figure 20 presents plots of horizontal and vertical flight paths obtained for velocities of 40, 60, 80, 100, 120, and 128 knots. The test altitude was 250 ft and the sideline and altitude deviation limits were set at ±20 ft (shown as straight solid lines in the figure). The direction of flight was from negative $x$ to positive $x$, and the average wind conditions at the test altitude were 15 mph from 260°. The microphone (mic) array is located from $x=0, y=0, z=0$ (position of reference mic) to $x=1000, y=0, z=0$. The upper plot presents the horizontal flight paths and shows that the aircraft was able to stay within the specified sideline deviation limits for all speeds although the winds tended to keep the aircraft toward the left of centerline. The lower plot presents the vertical flight tracks and shows that the aircraft was able to stay within the altitude deviation limits for all but the highest velocity case where the aircraft started at an altitude 10 ft below the lower altitude limit. However, the nominal directivity angle was still very small when the aircraft did enter the data box, thus resulting in a directivity-angle resolution that was significantly smaller than the maximum resolution angle. For this reason the flyover was judged acceptable.

Figure 21 presents plots of horizontal and vertical flight paths obtained for altitudes of 100, 250, 500, and 750 ft, respectively. The velocity was 80 knots and the altitude and sideline deviation limits for each altitude are listed in table III. Wind data at the test altitude were available for the 750-ft-altitude case only and were approximately 10 mph at 125°. For the other three altitudes presented, ground-weather-station wind data obtained from the top of a 10-m pole are presented in the figure and averaged 10 mph at 79°. The upper plot in each figure presents the horizontal flight paths and shows that the aircraft was able to remain within the sideline deviation limits for all altitudes. The lower plots present the horizontal flight paths and show that the aircraft exceeded the altitude deviation limits for three of the four altitudes presented. However, these limits were exceeded by a very small amount and at relatively small nominal directivity angles. This resulted in directivity-angle resolutions that were still significantly smaller than the maximum resolution angle. For this reason, these flyovers were all judged acceptable.

Figure 22 compares horizontal and vertical flight paths for gross weights of 2400 lb (dashed curve) and 3000 lb (solid curve). Figures 22(a) and 22(b) were obtained at an altitude of 250 ft and velocities of 80 and 120 knots, respectively, whereas figures 22(c) and 22(d) were obtained at an altitude of 750 ft and velocities of 80 and 120 knots, respectively. Average wind conditions at the test altitude are presented in each figure with the dashed line representing the winds for the 2400-lb case and the solid line representing the winds for the 3000-lb case. The upper plot in each figure presents the horizontal flight paths and shows that the aircraft was able to stay well within the sideline deviation limits for all cases except for the 80-knot, 750-ft-altitude case (fig. 22(c)). For this case the high winds just managed to push the aircraft outside the right sideline limit before the pilot was able to correct for it. Because this deviation was very small, however, the flyover was judged acceptable. The lower plots present the vertical flight paths and show that the aircraft was able to stay within the altitude deviation limits for all altitudes. The reduction in vehicle gross weight from 3000 to 2400 lb had no effect on the ability of the pilot to keep the aircraft within the altitude and sideline deviation limits.

Figure 23 compares horizontal and vertical flight paths for main rotor rotational speeds ($N_2$) of 103 percent (solid curve) and 90 percent (dashed curve). The normal operating speed of $N_2$ is 103 percent. Figures 23(a) and 23(b) were obtained at an altitude of 250 ft and velocities of 80 and 120 knots, respectively, while figures 23(c) and 23(d) were obtained at an altitude of 750 ft and velocities of 80 and 120 knots, respectively. Average wind conditions at the test altitude are presented in each figure with the dashed line representing the winds for the 90-percent $N_2$ case and the solid line representing the winds for the 103-percent $N_2$ case. The upper plot in each figure presents the horizontal flight paths and shows that the aircraft was able to stay well within the sideline deviation limits for all rotor speeds. The lower plots present the vertical flight path and show that the aircraft was able to stay within the altitude deviation limits for all cases except the 120-knot, 750-ft-altitude flyover (fig. 23(d)). For this case the aircraft suddenly began to increase in altitude and barely exceeded the upper altitude limit before the pilot was able to correct for it. Because this deviation was very small, however, the flyover was judged acceptable. The reduction in main rotor rotational speed from 103- to 90-percent $N_2$ had no apparent effect on the ability of the pilot to keep the aircraft within the altitude and sideline deviation limits.

Following are some general observations of the ability of the aircraft to maintain the desired flight path. First, it should be emphasized that during

every run the aircraft pilot was in constant communication with a radar technician who was guiding him through the box created by the altitude and sideline deviation limits (as described in the "Acoustic Instrumentation and Flight Test Procedures" section). Also, it should be pointed out that two flyovers were typically required at each condition to obtain an acceptable flight path. Maintaining the proper altitude seemed to be more difficult than maintaining the proper horizontal path since the pilot can use visual ground references to horizontally align the aircraft flight path. Visual ground referencing becomes less accurate with increasing altitude, thereby necessitating the expansion of the altitude and sideline deviation limits. As the aircraft velocity increases, the pilot must react more quickly to any deviations from the desired flight path caused by wind gusts, etc., in order to stay within the altitude and sideline deviation limits. Finally, during this flight test program, the ratio of acceptable flyovers to total number of flyovers increased dramatically with pilot experience, thus indicating that practice is extremely valuable.

### Variability of Aircraft Attitude

The acoustic analysis assumes that the aircraft not only flies a straight-and-level path, but also flies with a heading that is always aligned exactly in the desired direction with a pitch attitude of 0°. Figure 24 presents the aircraft heading and pitch attitude for velocities of 40, 60, 80, 100, 120, and 128 knots at a 250-ft altitude for the flight paths presented in figure 20. The direction of flight was from negative $x$ to positive $x$, and the average wind conditions at the test altitude were approximately 15 mph at 260°. The desired flight path heading was 100°.

The upper plot in figure 24 presents the aircraft heading as a function of distance from the reference microphone and shows that due to the prevailing wind conditions, a yaw or crab angle of as much as 20° was required to maintain the desired flight path. The 40-knot flyover required the greatest crab angle, whereas the 100-knot flyover required the smallest crab angle. The expected result of decreasing crab angle with increasing velocity does not hold in this velocity sweep, probably because of varying wind conditions. Although the 40-, 60-, 100-, and 128-knot runs were all obtained within a 20-minute span, the 80- and 120-knot runs were obtained approximately 1 hour earlier. At only one instant was the aircraft heading actually aligned with the desired direction of flight (the 100-knot flyover at approximately 2900 ft). The lower plot presents the aircraft pitch attitude as a function of distance from the reference microphone and shows that, as expected for a helicopter, the pitch attitude decreases with increasing velocity. For this velocity range the aircraft pitch attitude varied from about 4° to −6°, but it held within about ±2° for a typical run. This figure shows that the aircraft attitude must be considered when determining the lower hemispherical acoustic signature from an aircraft flyover.

## Concluding Remarks

A study was conducted to investigate the measurement resolution of noise directivity patterns from acoustic flight tests. Directivity-angle resolution is affected by the data reduction parameters, the aircraft velocity and flyover altitude, and deviations of the aircraft from the desired flight path. The maximum directivity-angle resolution typically occurs when the aircraft is at or near the overhead position. The maximum longitudinal-directivity-angle resolution is affected by all the above parameters, whereas the maximum lateral-directivity-angle resolution is affected by altitude only. In general, directivity-angle resolution improves with decreasing velocity, increasing altitude, increasing sampling rate, decreasing block size, and decreasing block averages. Deviations from the desired ideal flight path will increase the resolution.

At the typical test altitude of 250 ft, sideline and altitude deviation limits of ±20 ft were selected and the flyover distance for acoustic data acquisition was approximately 7500 ft. On average, two flyovers were required at each test condition to obtain an acceptable flight path. The ability of the pilot to maintain the flight path improved with decreasing altitude, decreasing velocity, and practice. As a result of the prevailing wind conditions, yaw angles of as much as 20° were required to maintain the desired flight path. Helicopter pitch attitude typically varied ±2° during a flyover.

NASA Langley Research Center
Hampton, VA 23665-5225
August 4, 1989

## References

1. Leverton, John W.: An Overview of Helicopter's Environmental Considerations. *Vertiflite,* vol. 31, no. 1, Jan./Feb. 1985, pp. 14–15.
2. Leverton, John W.: Aeroacoustics Historical Prospective and Important Issues. *National Specialists' Meeting on Aerodynamics and Aeroacoustics - Proceedings,* American Helicopter Soc., c.1987.
3. Foster, Charles R.: Helicopter External Noise Requirements- FAA Perspective. *Helicopter Acoustics,* NASA CP-2052, Part I, 1978, pp. 1–16.

4. Powell, Clemans A.; and McCurdy, David A.: *Effects of Repetition Rate and Impulsiveness of Simulated Helicopter Rotor Noise on Annoyance.* NASA TP-1969, 1982.
5. Golub, Robert A.; and Weir, Donald S.: The Phase II ROTONET System. *National Specialists' Meeting on Aerodynamics and Aeroacoustics – Proceedings,* American Helicopter Soc., c.1987.
6. Morse, Philip M.; and Ingard, K. Uno: *Theoretical Acoustics.* McGraw-Hill Book Co., Inc., c.1968.
7. *American National Standard Method for the Calculation of the Absorption of Sound by the Atmosphere.* ANSI SI.26-1978 (ASA 23-1978), American Inst. of Physics, 1978.
8. Gridley, Doreen: *Program for Narrow-Band Analysis of Aircraft Flyover Noise Using Ensemble Averaging Techniques.* NASA CR-165867, 1982.
9. Thomas, Mitchel E.; and Diamond, John K.: Application of Low-Power, High-Rate PCM Telemetry in a Helicopter Instrumentation System. *Proceedings of the 33rd International Instrumentation Symposium,* Instrument Soc. of America, c.1987, pp. 383–397.
10. Sentell, Ronald J.; Storey, Richard W.; Chang, James J. C.; and Jacobson, Stephen J.: *Tethered Balloon-Based Measurements of Meteorological Variables and Aerosols.* NASA TM X-73999, 1976.
11. Bendat, Julius S.; and Piersol, Allan G.: *Random Data Analysis and Measurement Procedures, Second ed.* (Revised and Expanded). John Wiley & Sons, Inc., c.1986.
12. Hardin, Jay C.: *Introduction to Time Series Analysis.* NASA RP-1145, 1986.
13. Dahan, Claude; and Gratieux, Edmond: Helicopter Rotor Thickness Noise. *J. Aircr.,* vol. 18, no. 6, June 1981, pp. 487–494.

Table I. HIARS Measurement List for 500E Flight Test Program

| Parameter | Sampling rate, samples per sec | Range |
|---|---|---|
| **Rotating blade measurements** | | |
| Flapping angle | 5555 | 0° to 20° max. |
| Lead-lag angle | 5555 | 15° to 5° max. |
| Feathering angle | 5555 | −17° to 32° max. |
| **Nonrotating blade measurements** | | |
| MR collective | 231 | 0° to 15° |
| TR collective | 231 | −13° to 27° |
| Longitudinal cyclic | 231 | 17° forward to 7° aft |
| Lateral cyclic | 231 | 7° port to 5.5° starboard |
| MR, 1/rev | 5555 | 550 rpm max. |
| TR, 1/rev | 231 | 3275 rpm max. |
| MR, 256/rev | 5555 | 550 rpm max. |
| **Engine and gearbox measurements** | | |
| Exhaust gas temperature (TOT) | 231 | 0°C to 1000°C |
| $N_1$ | 231 | 65 000 rpm max. |
| $N_2$ | 231 | 6800 rpm max. |
| $N_R$ | 231 | 550 rpm max. |
| Torque | 231 | 0 to 100 psia |
| Fuel totalizer | 231 | |
| Fuel flow | 231 | 150 gal/hr max. |
| Fuel temperature | 231 | |
| **Helicopter state measurements** | | |
| Airspeed | 231 | 30 to 200 knots |
| Altitude | 231 | 0 to 2000 ft |
| Altitude rate | 231 | 0 to 1200 ft/min |
| Angle of attack | 231 | ±15° |
| Angle of sideslip | 231 | ±30° |
| Ambient pressure | 231 | 1900 to 2150 psf |
| Ambient temperature | 231 | 30°F to 100°F |
| Roll altitude | 231 | ±90° |
| Roll altitude rate | 231 | 60 deg/sec |
| Yaw altitude | 231 | 0° to 360° |
| Yaw altitude rate | 231 | 60 deg/sec |
| Pitch altitude | 231 | ±30° |
| Pitch altitude rate | 231 | 60 deg/sec |

Table II. Typical 500E Conditions and Variations Used in Parametric Studies

| Parameter | Typical 500E conditions | Variations used in parametric studies |
|---|---|---|
| Velocity, knots | 80 | 40 140 |
| Altitude, ft | 250 | 100 750 |
| Altitude deviation limits, ft | ±20 | |
| Sideline deviation limits, ft | ±20 | |
| Data digitization rate, samples per second | 25 000 | 15 000 40 000 |
| FFT block size, samples | 2048 | 512 4096 |
| Number of FFT blocks used in ensemble average | 5 | 1 9 |

Table III. Altitude and Sideline Deviation Limits Selected for 500E Flight Test Program With Magnitude and Location of Associated Maximum Directivity-Angle Resolutions

| Altitude, ft | Altitude and sideline deviation limits, ft | Maximum longitudinal-directivity-angle resolution | | Maximum lateral-directivity-angle resolution | |
|---|---|---|---|---|---|
| | | Amplitude, deg | Nominal directivity angles for maximum resolution angle, deg | Amplitude, deg | Nominal directivity angles for maximum resolution angle, deg |
| 100 | ±10 | 33 | 90 | 11 | $75 \leq \theta \leq 105$ |
| 250 | ±20 | 14 | 72, 108 | 9 | $84 \leq \theta \leq 96$ |
| 500 | ±30 | 8 | 67, 113 | 7 | $87 \leq \theta \leq 93$ |
| 750 | ±40 | 6 | 62, 118 | 6 | $88 \leq \theta \leq 92$ |

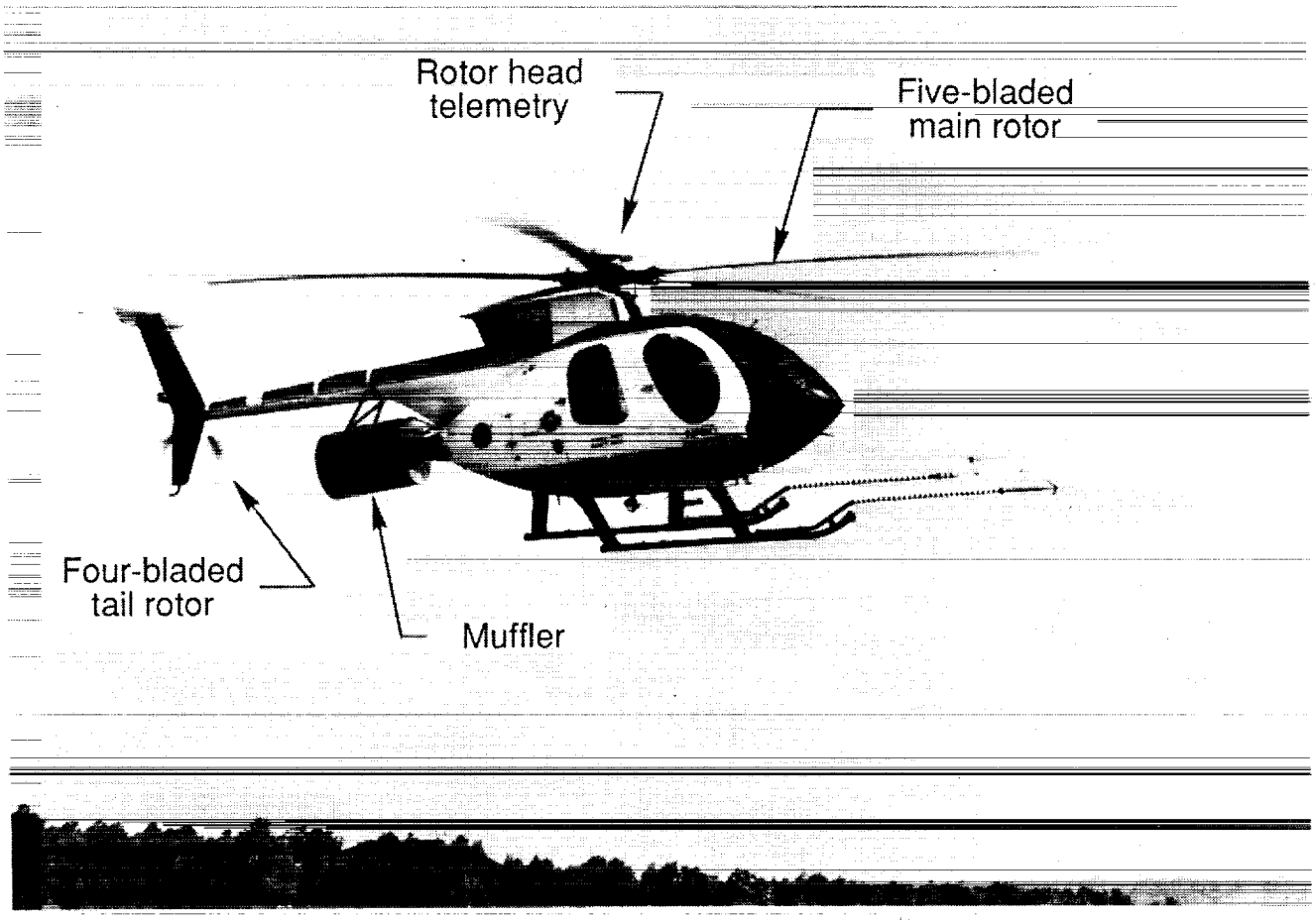


Figure 1. The McDonnell Douglas 500E experimental helicopter.

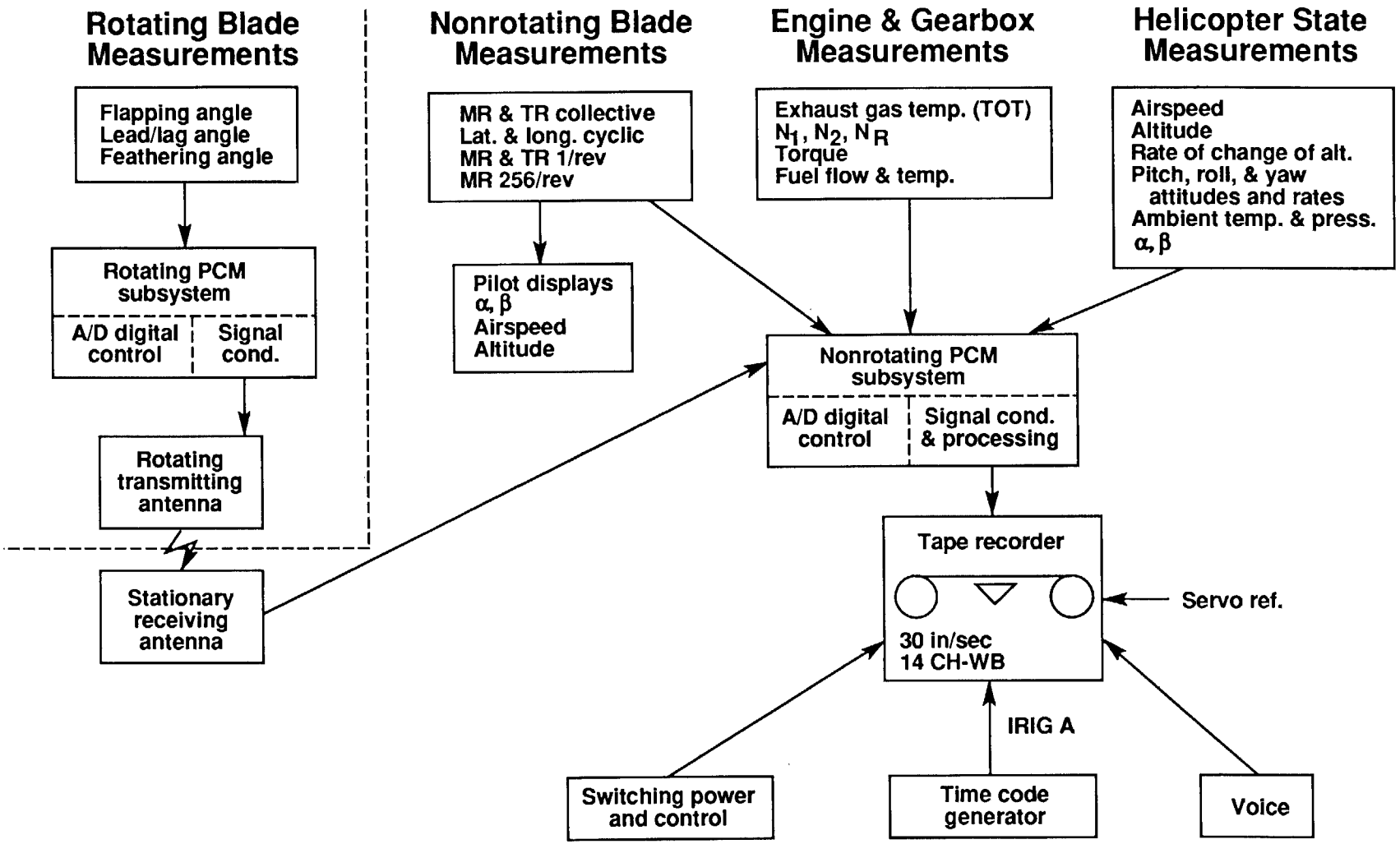


Figure 2. HIARS system schematic.

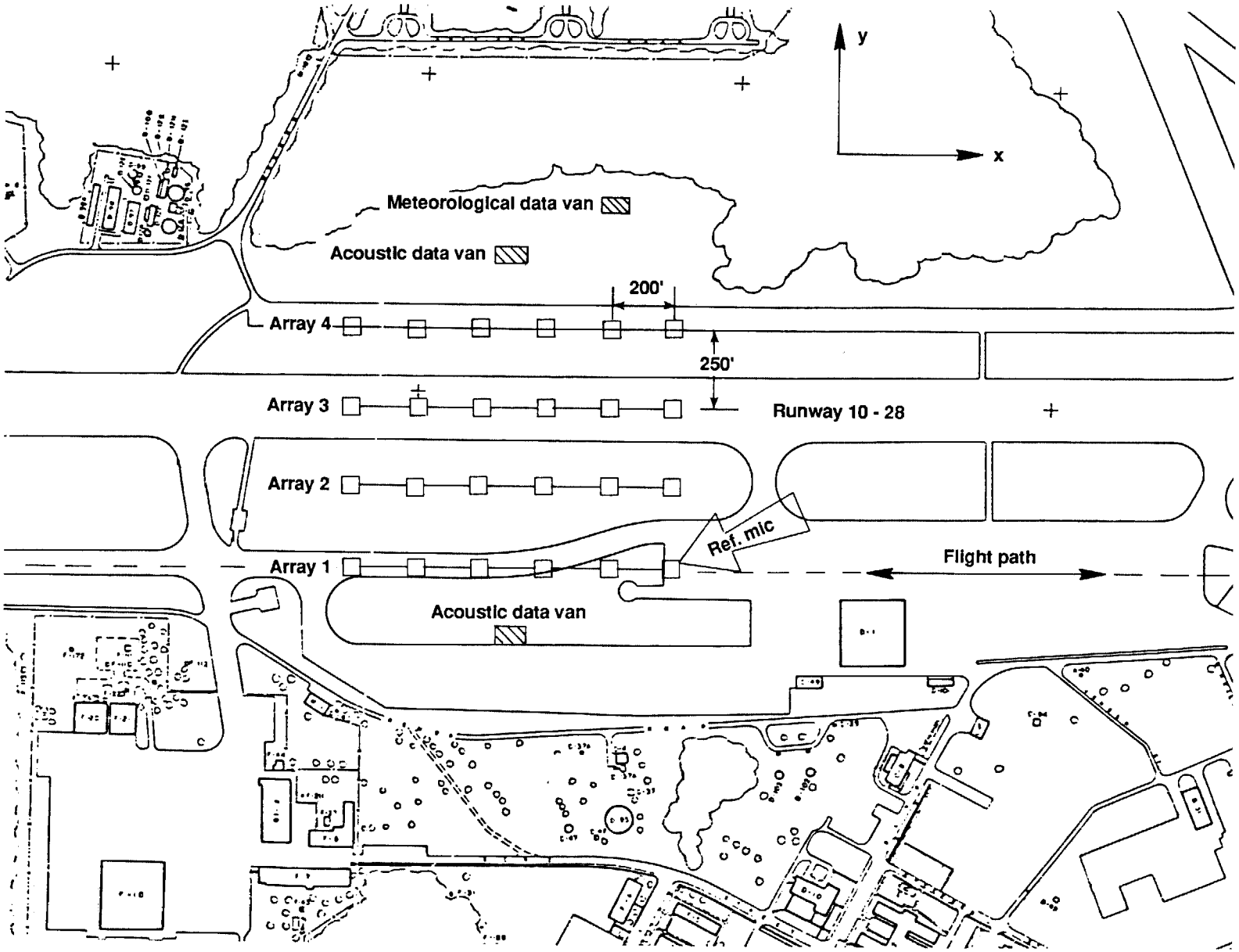


Figure 3. Microphone array. Reference microphone is the coordinate system origin ($x = y = z = 0$).

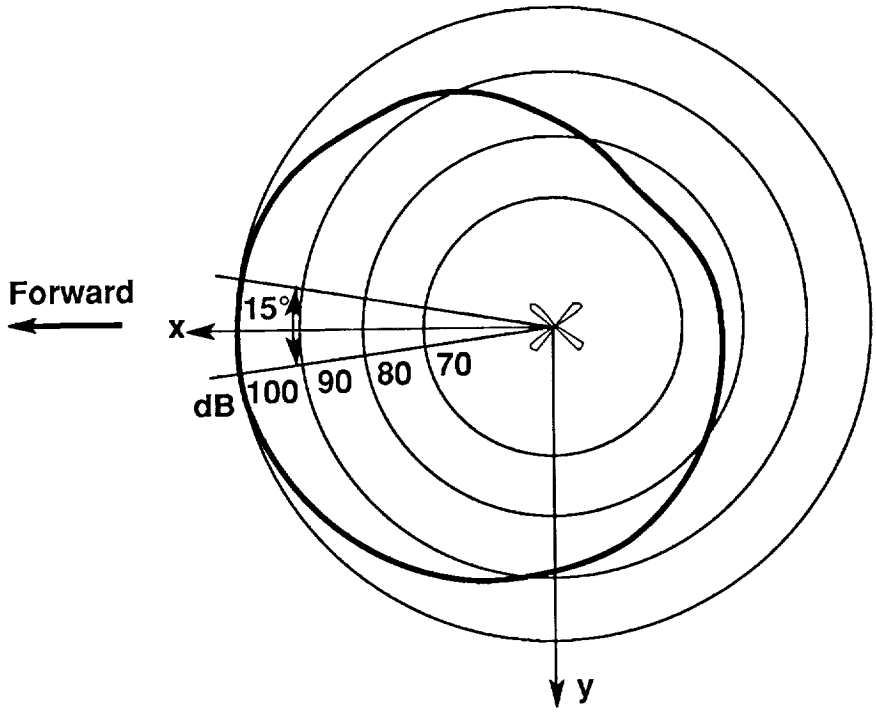


(a) Horizontal directivity pattern.

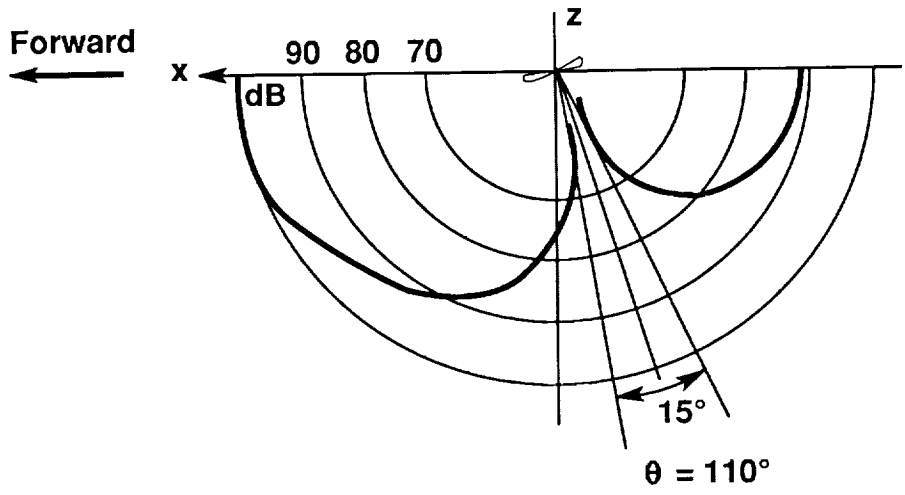


(b) Vertical directivity pattern.

Figure 4. Predicted acoustic directivity pattern of main rotor thickness noise. $\Omega$ = 450 rpm; $V$ = 140 knots.

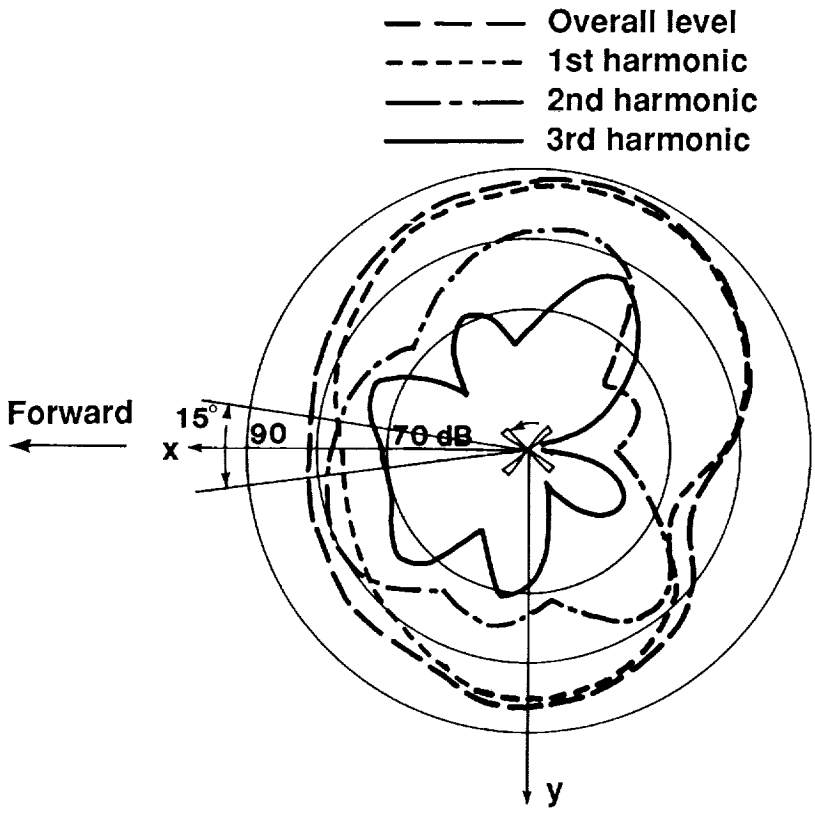


(a) Horizontal directivity pattern.

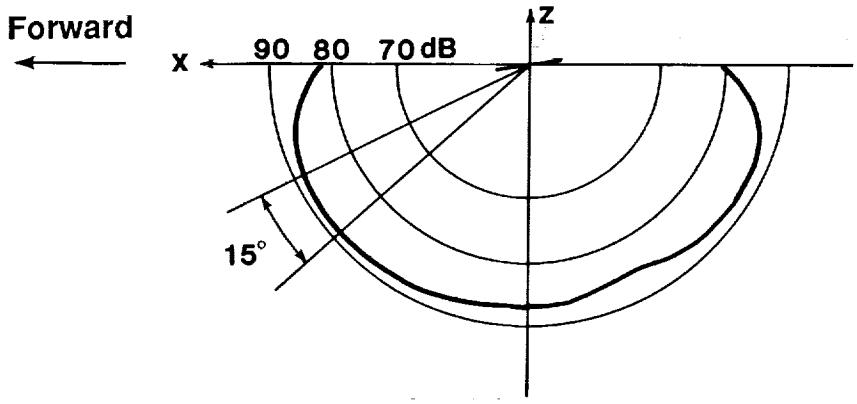


(b) Vertical directivity pattern.

Figure 5. Predicted acoustic directivity pattern of main rotor loading noise. $\Omega = 350$ rpm; $V = 140$ knots.

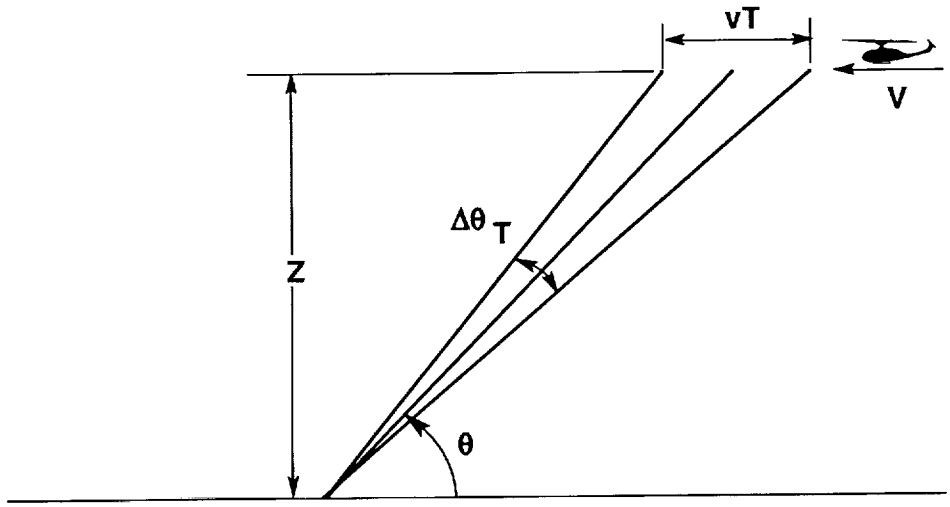


(a) Definition of variables used in equation (3).

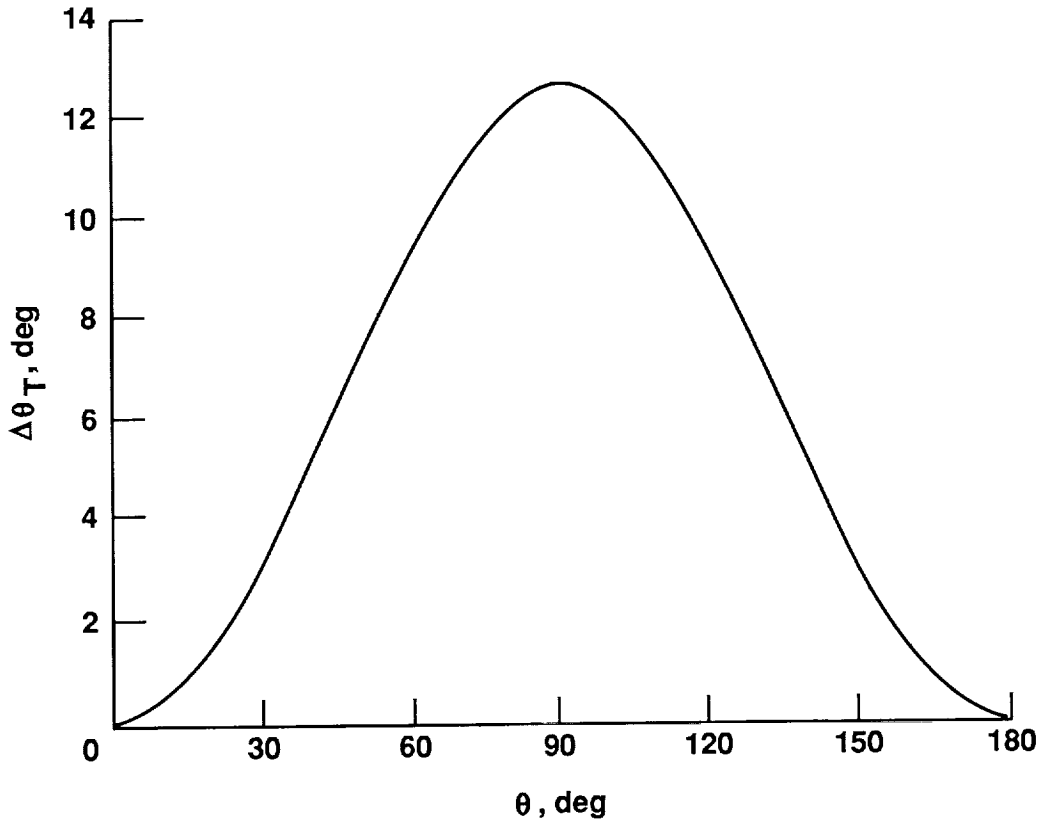


(b) Variation of directivity-angle resolution with nominal directivity angle. $V = 80$ knots; $Z = 250$ ft; SR = 25 kHz; $b = 2048$; $N_B = 5$.

Figure 6. Longitudinal-directivity-angle resolution due to block averaging.

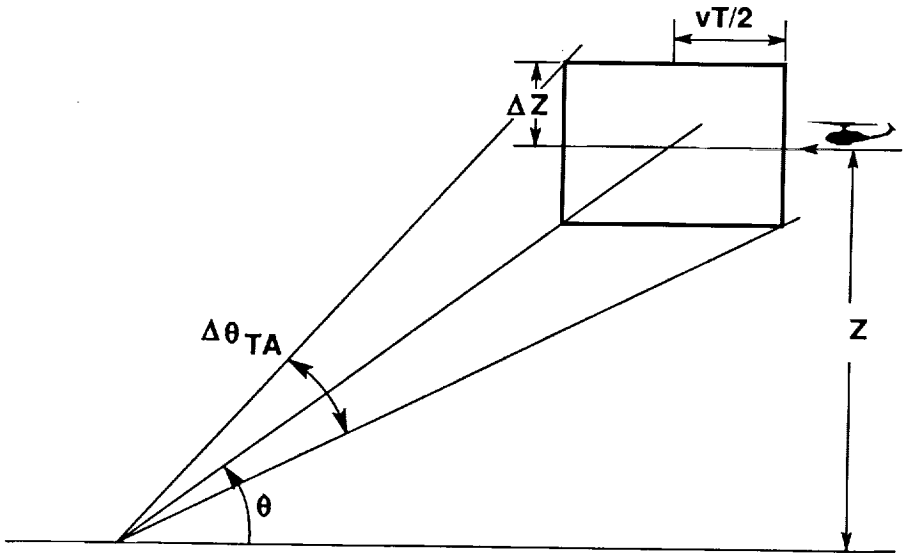


(a) Definition of variables used in equations (6), (7), and (8).

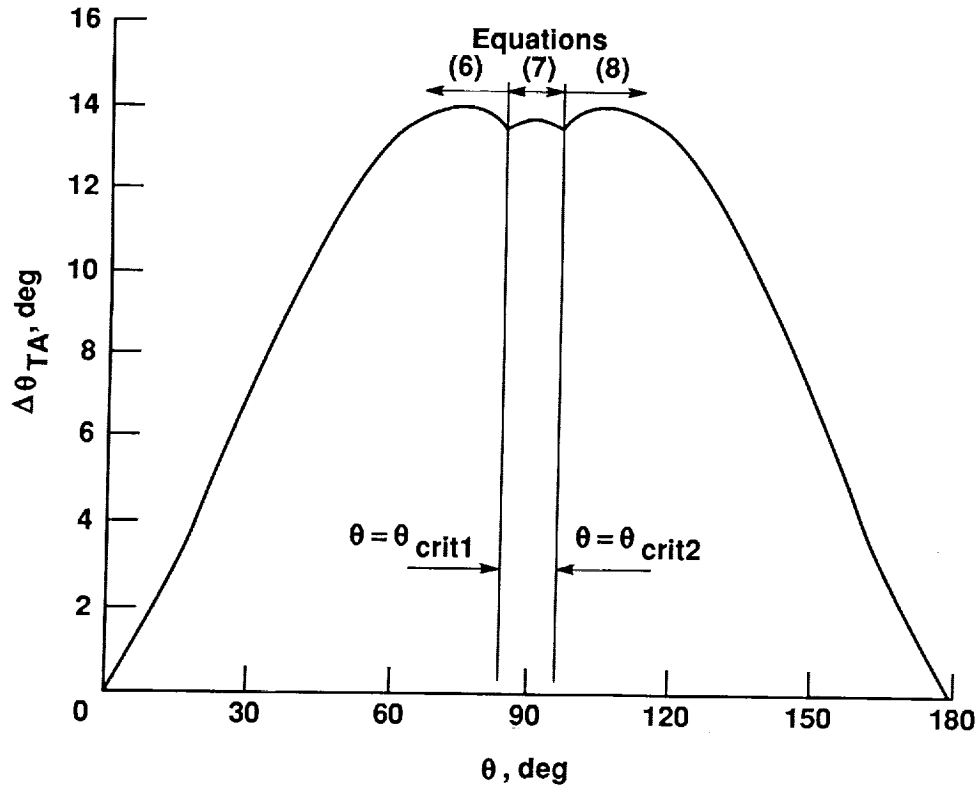


(b) Variation of maximum directivity-angle resolution with nominal directivity angle. $V = 80$ knots; $Z = 250$ ft; $\Delta Z = \pm 20$ ft; SR = 25 kHz; $b = 2048$; $N_B = 5$.

Figure 7. Maximum longitudinal-directivity-angle resolution due to combined effects of block averaging and altitude deviation limits.

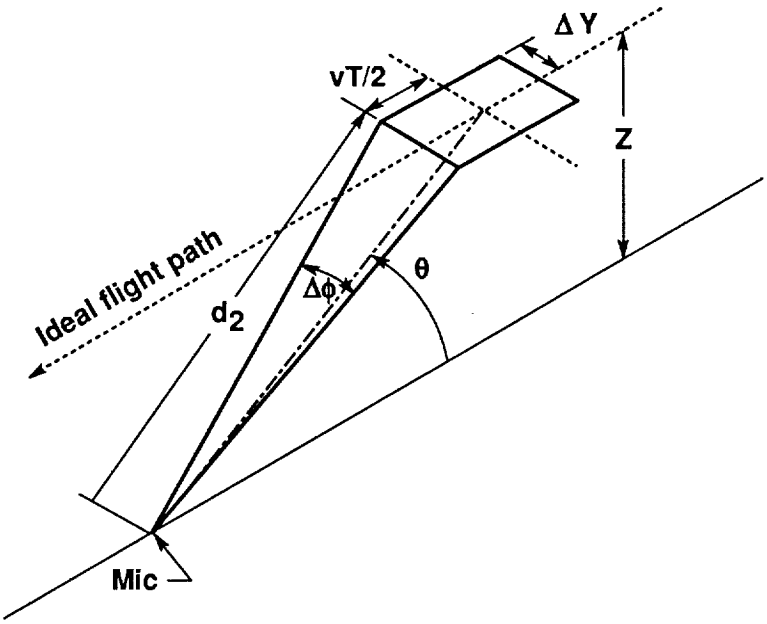


(a) Definition of variables used in equations (9), (10), and (11).

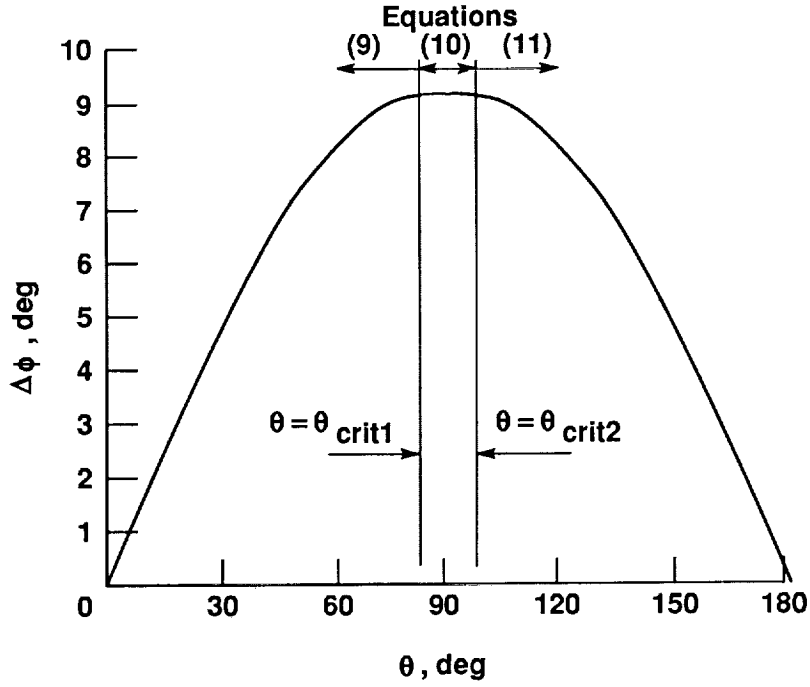


(b) Variation of maximum directivity-angle resolution with nominal directivity angle. $V = 80$ knots; $Z = 250$ ft; $\Delta Y = \pm 20$ ft; SR = 25 kHz; $b = 2048$; $N_B = 5$.

Figure 8. Maximum lateral-directivity-angle resolution due to sideline deviation limits.

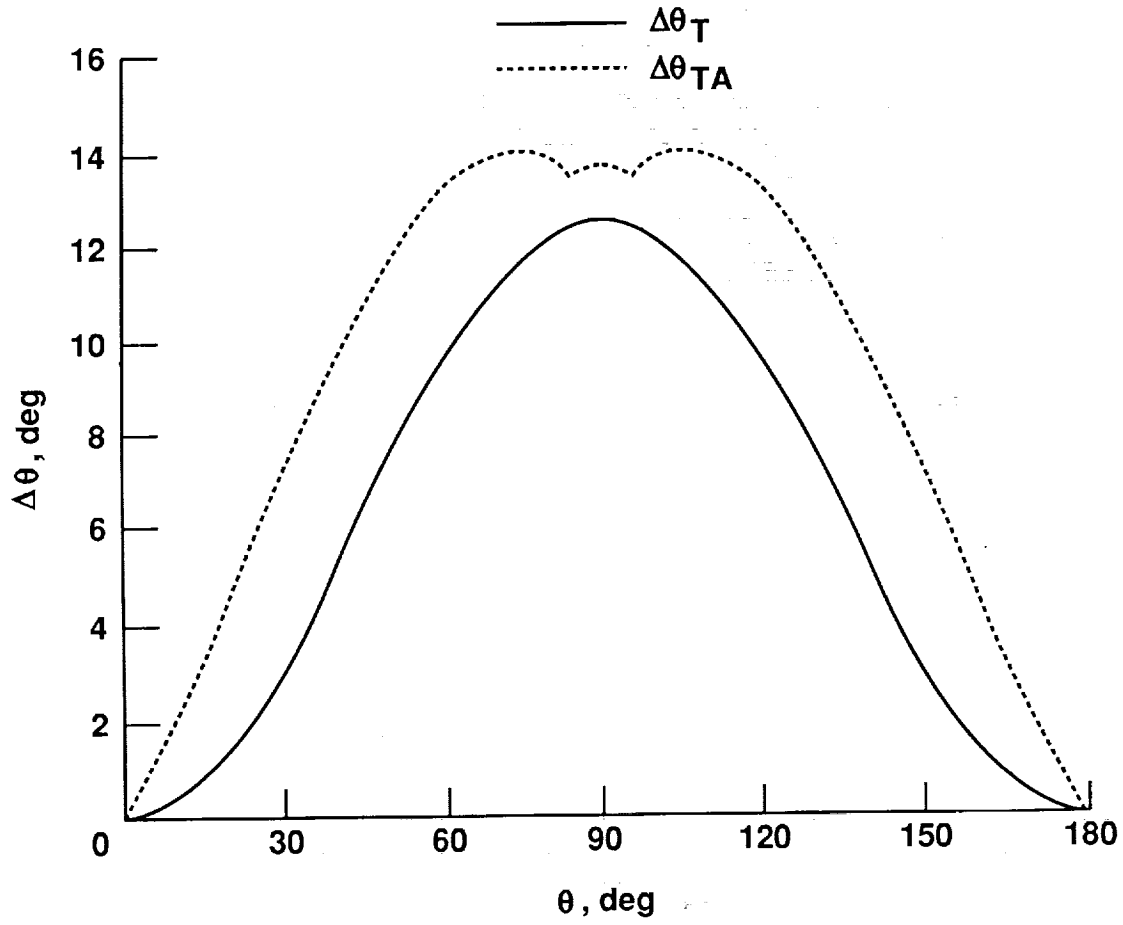


Figure 9. Longitudinal-directivity-angle resolution boundaries. $V = 80$ knots; $Z = 250$ ft; $\Delta Y = \Delta Z = \pm 20$ ft; SR = 25 kHz; $b = 2048$; $N_B = 5$.

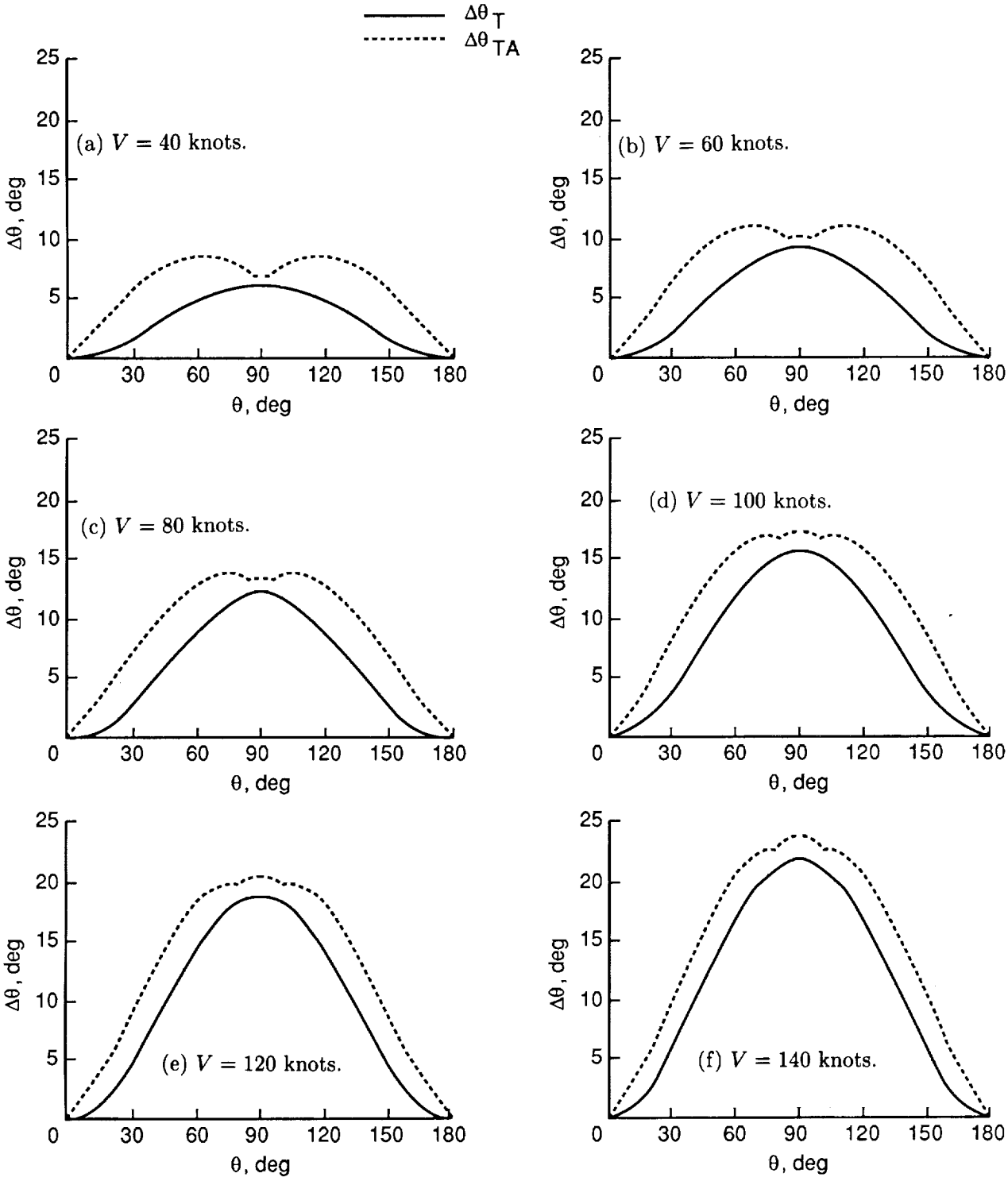


Figure 10. Longitudinal-directivity-angle resolution boundaries for range of velocities. $Z$ = 250 ft; $Z$ = 20 ft; SR = 25 kHz; $b$ = 2048; $N_B$ = 5.

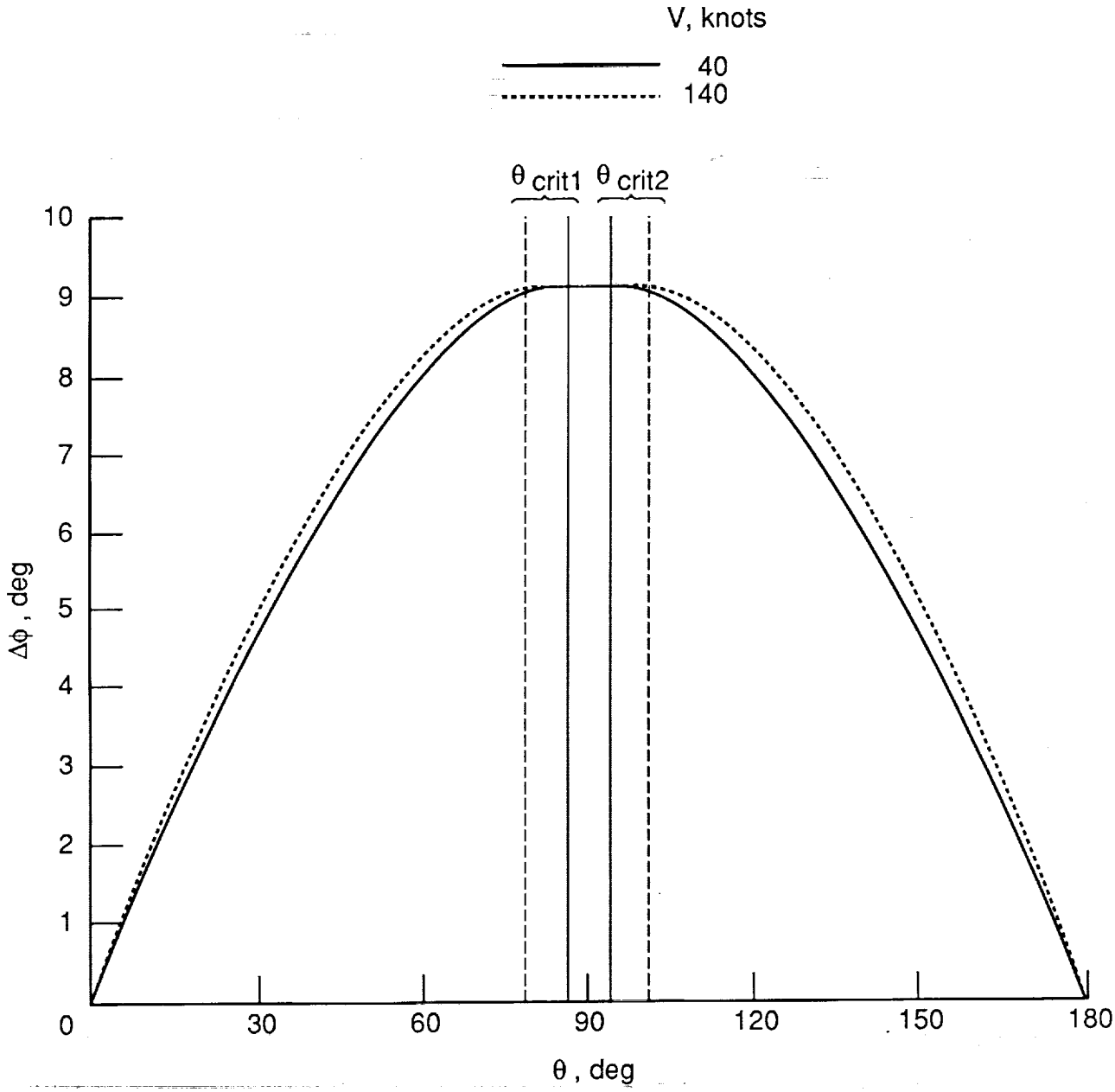


Figure 11. Lateral-directivity-angle resolution boundaries for range of velocities. $Z = 250$ ft; $\Delta Y = \pm 20$ ft; SR = 25 kHz; $b = 2048$; $N_B = 5$.

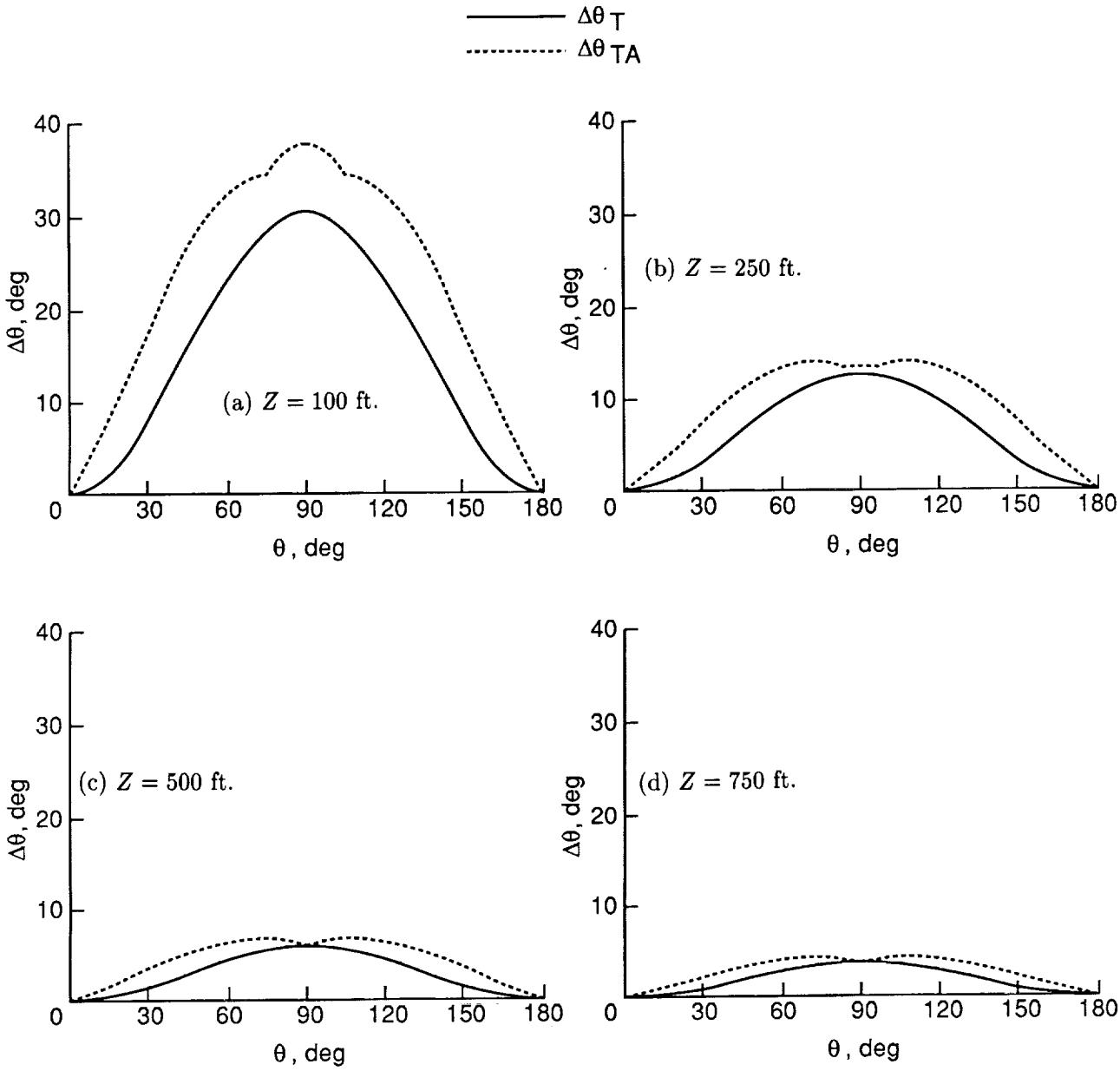


Figure 12. Longitudinal-directivity-angle resolution boundaries for range of altitudes. $V = 80$ knots; $\Delta Z = \pm 20$ ft; SR = 25 kHz; $b = 2048$; $N_B = 5$.

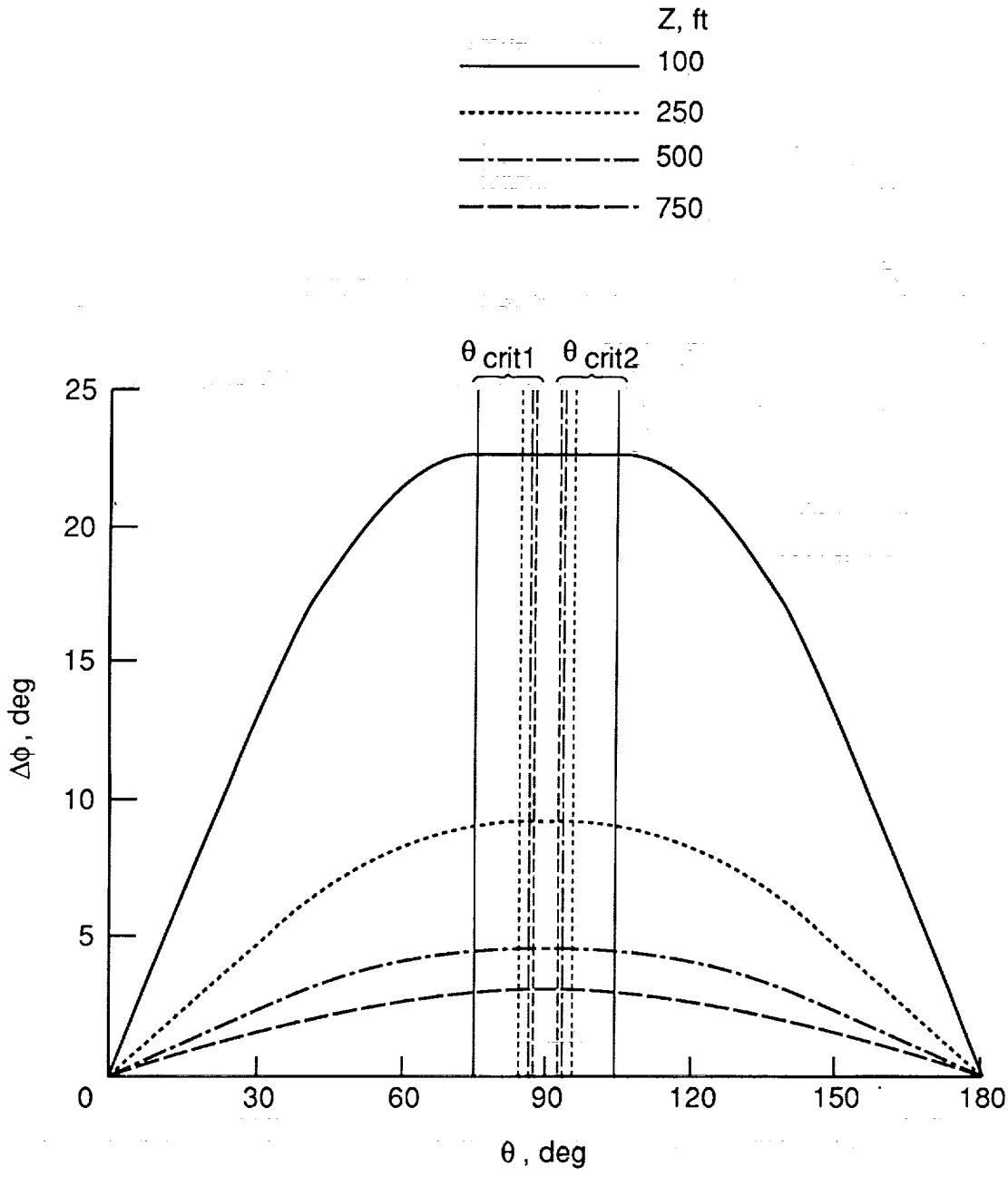


Figure 13. Lateral-directivity-angle resolution boundaries for range of altitudes. $V = 80$ knots; $\Delta Y = \pm 20$ ft; SR = 25 kHz; $b = 2048$; $N_B = 5$.

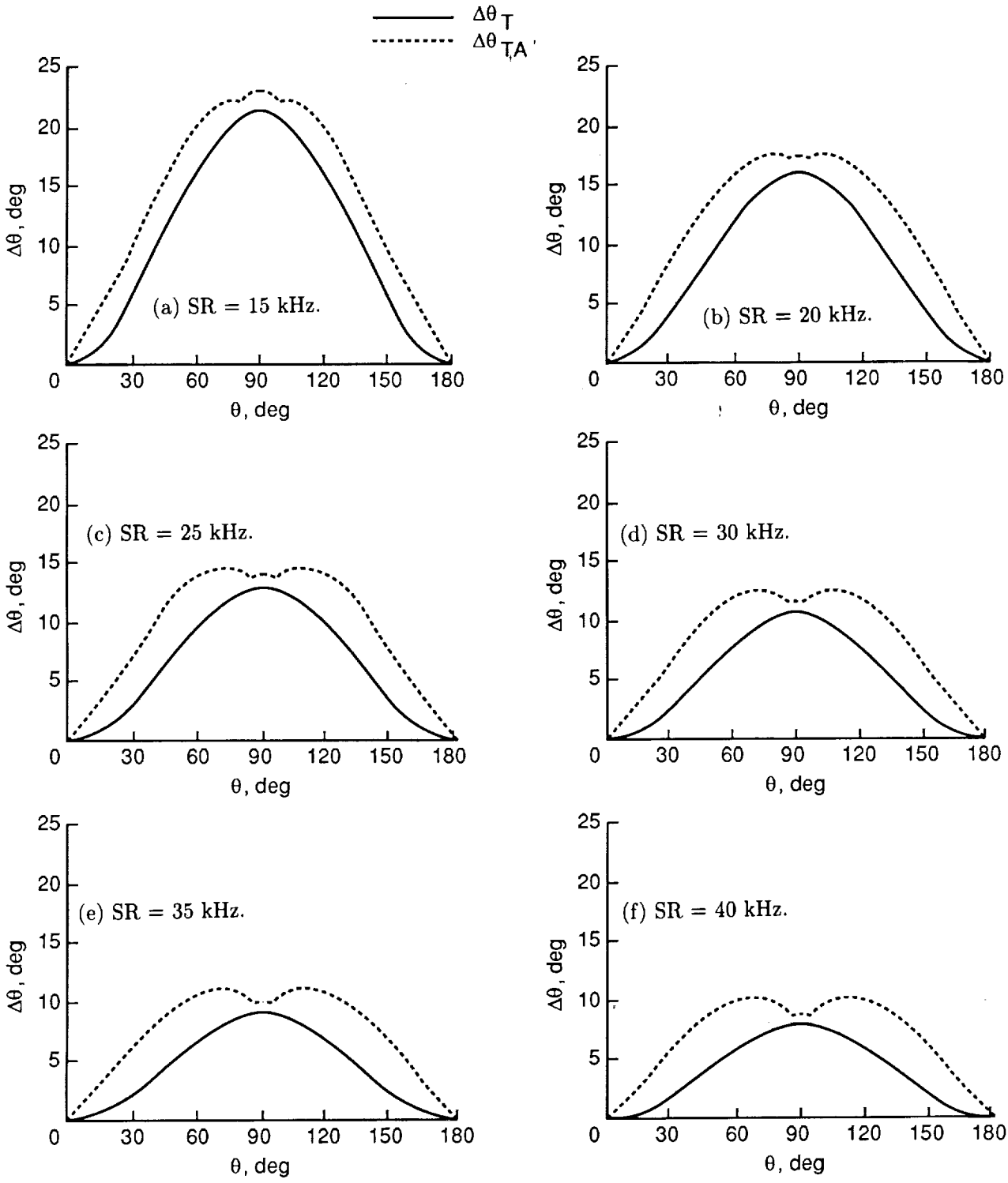


Figure 14. Longitudinal-directivity-angle resolution boundaries for range of sampling rates. $V = 80$ knots; $Z = 250$ ft; $\Delta Z = \pm 20$ ft; $b = 2048$; $N_B = 5$.

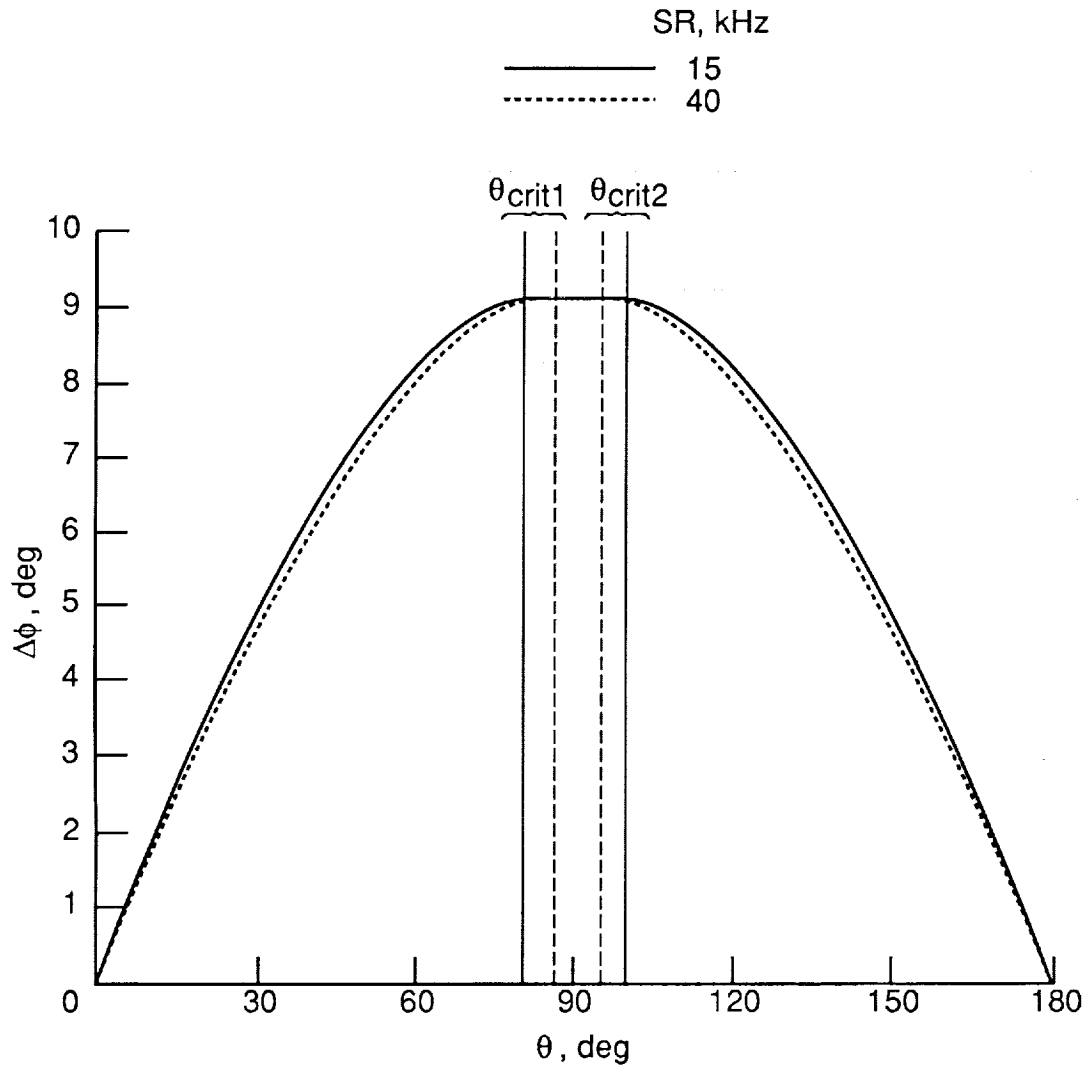


Figure 15. Lateral-directivity-angle resolution boundaries for range of sampling rates. $V = 80$ knots; $Z = 250$ ft; $\Delta Y = \pm 20$ ft; $b = 2048$; $N_B = 5$.

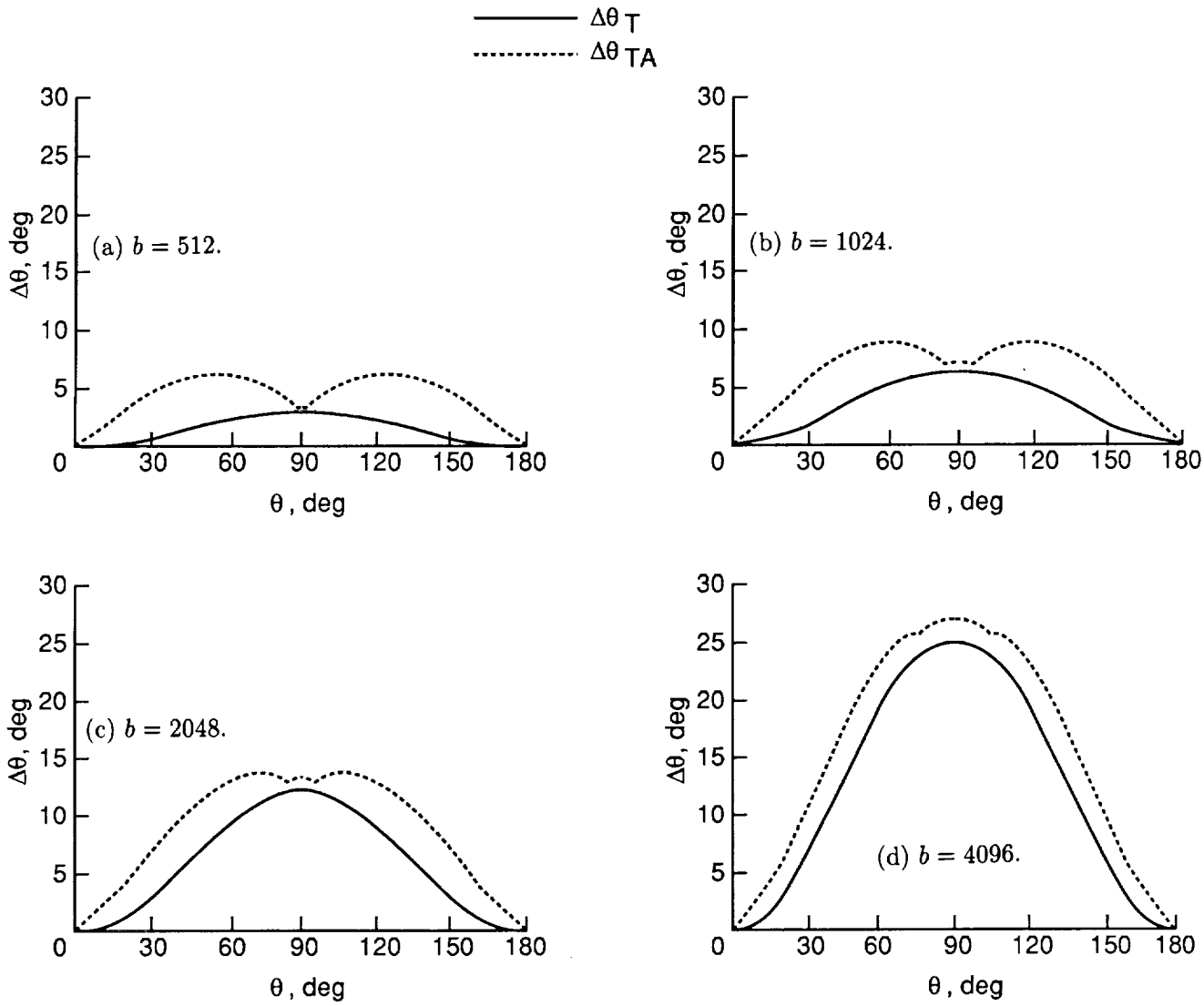


Figure 16. Longitudinal-directivity-angle resolution boundaries for range of transform sizes. $V = 80$ knots; $Z = 250$ ft; $\Delta Z = \pm 20$ ft; SR = 25 kHz; $N_B = 5$.

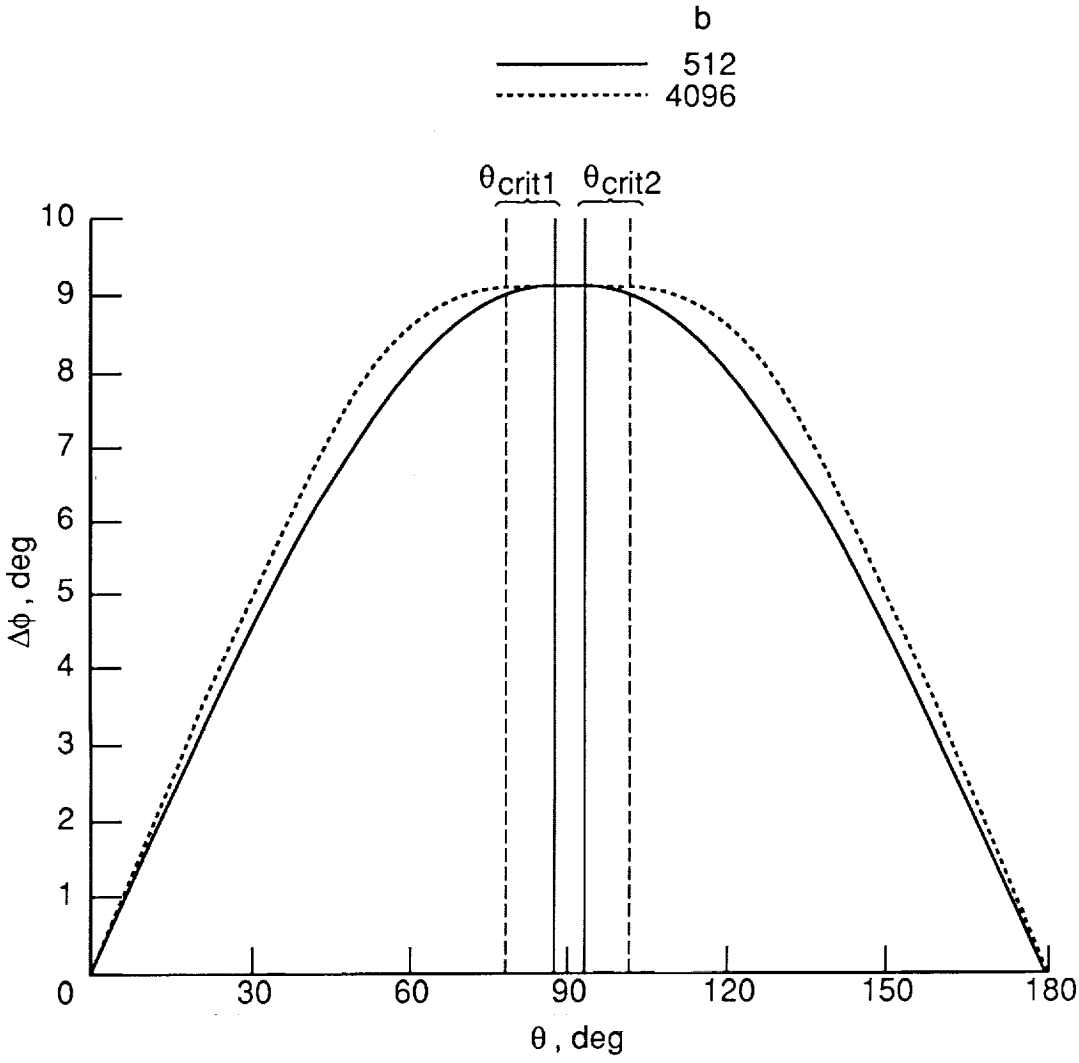


Figure 17. Lateral-directivity-angle resolution boundaries for range of transform sizes. $V = 80$ knots; $Z = 250$ ft; $\Delta Y = \pm 20$ ft; SR = 25 kHz; $N_B = 5$.

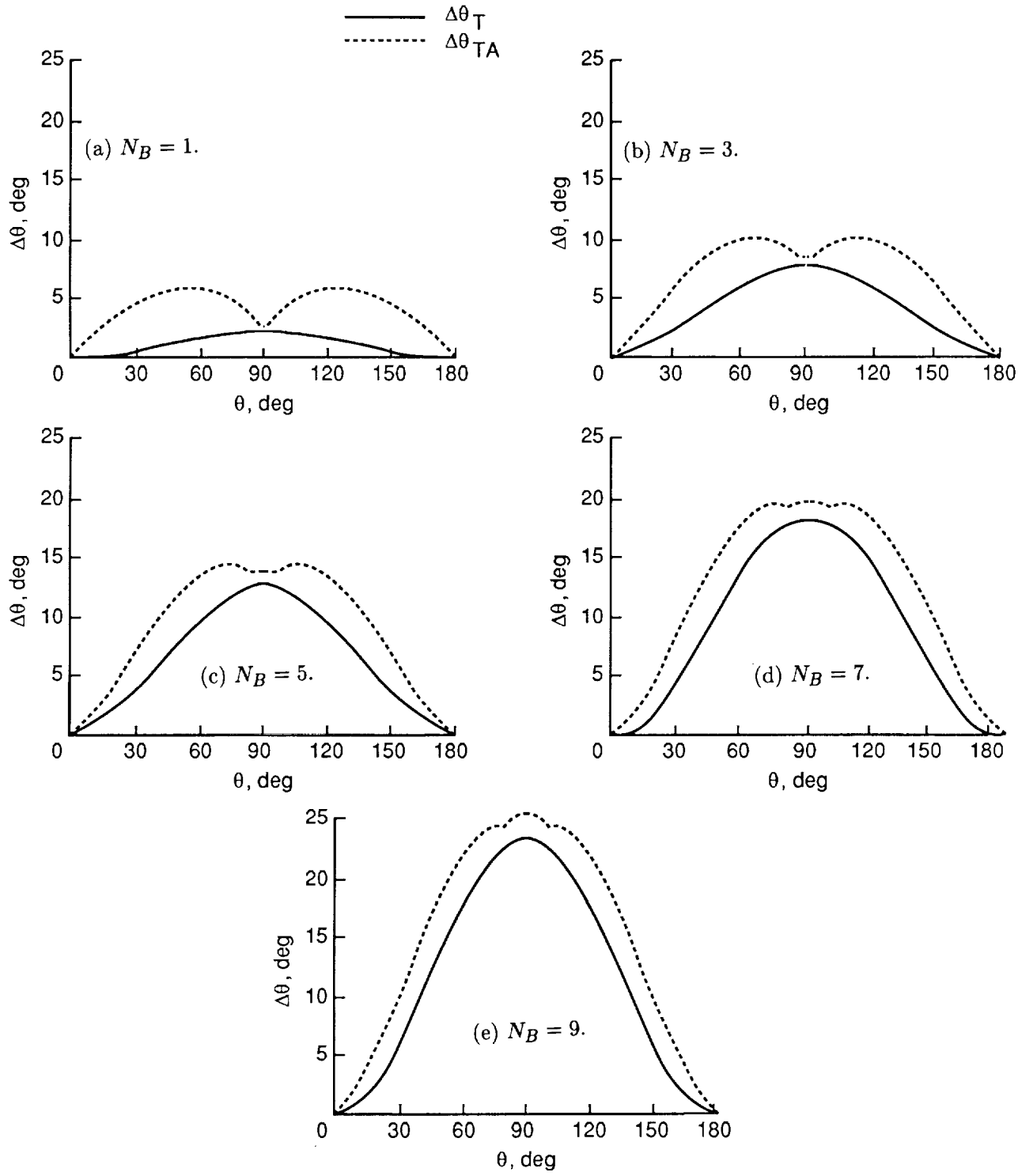


Figure 18. Longitudinal-directivity-angle resolution boundaries for range of transform averages. $V$ = 80 knots; $Z$ = 250 ft; $\Delta Z = \pm 20$ ft; SR = 25 kHz; $b$ = 2048.

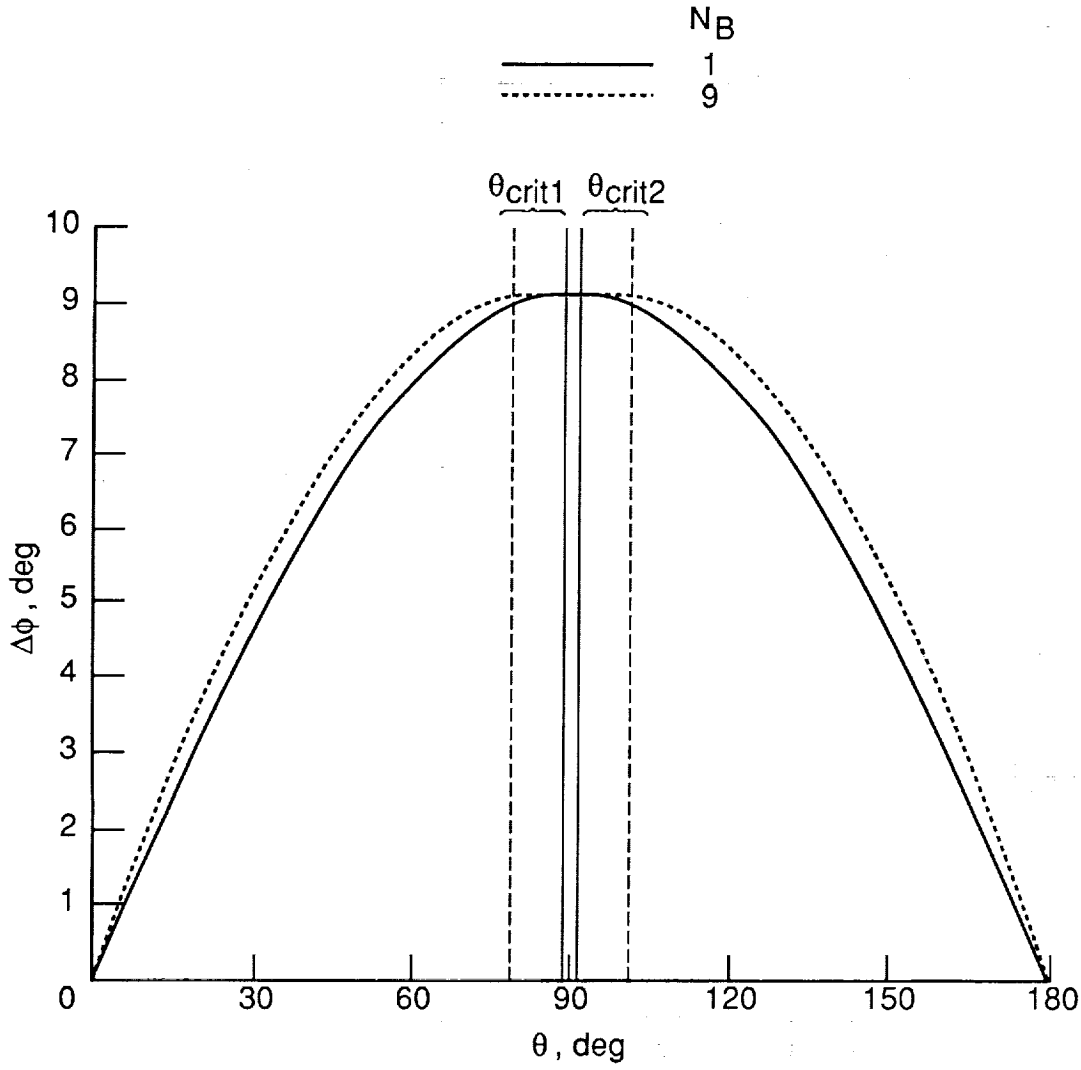


Figure 19. Lateral-directivity-angle resolution boundaries for range of transform averages. $V = 80$ knots; $Z = 250$ ft; $\Delta Y = \pm 20$ ft; SR = 25 kHz; $b = 2048$.

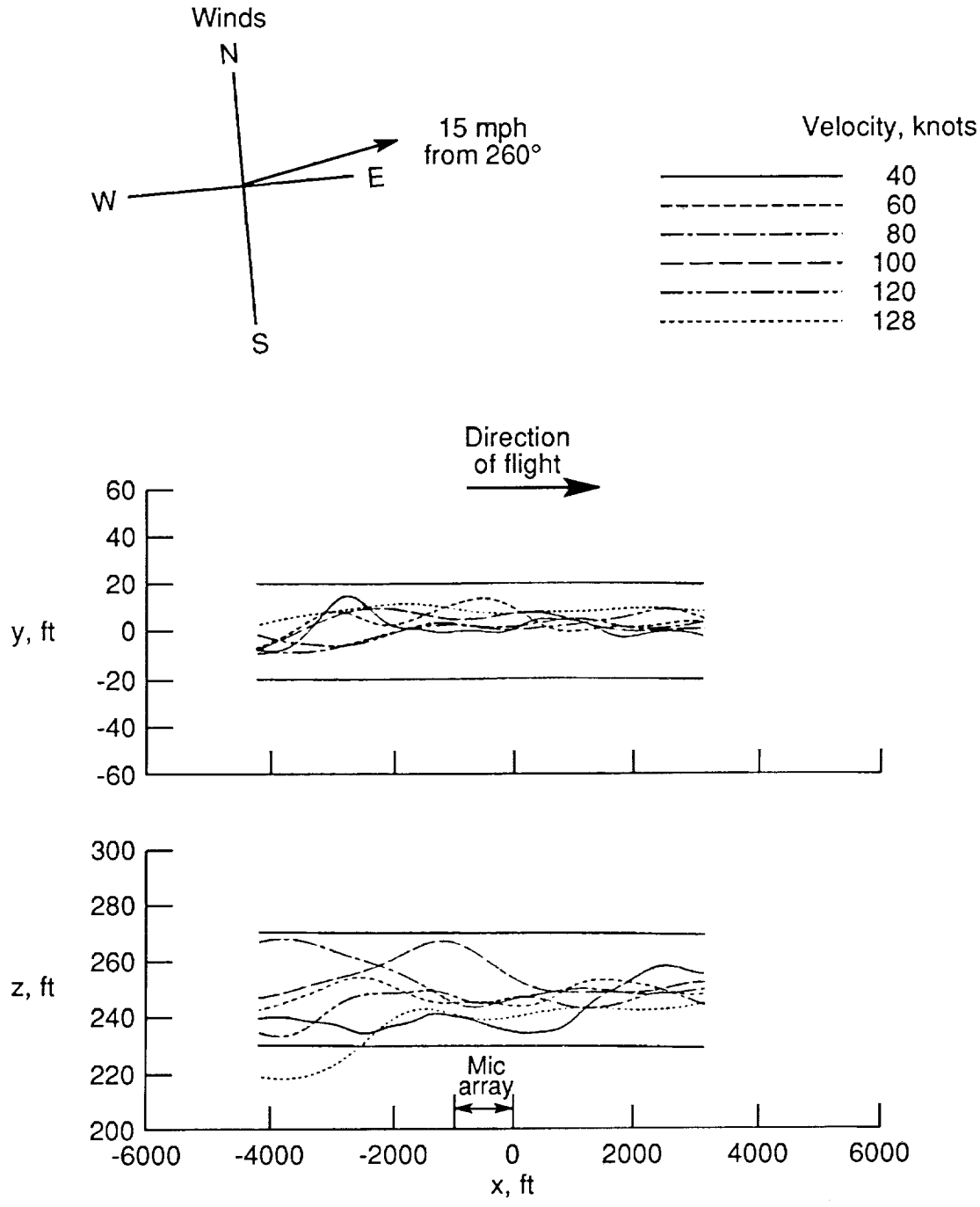


Figure 20. Effect of velocity on vertical and horizontal flight paths from 500E flight test program. Two-bladed TR; Gross weight = 3000 lb; $N_2$ = 103 percent; $Z$ = 250 ft; $\Delta Y = \pm 20$ ft.

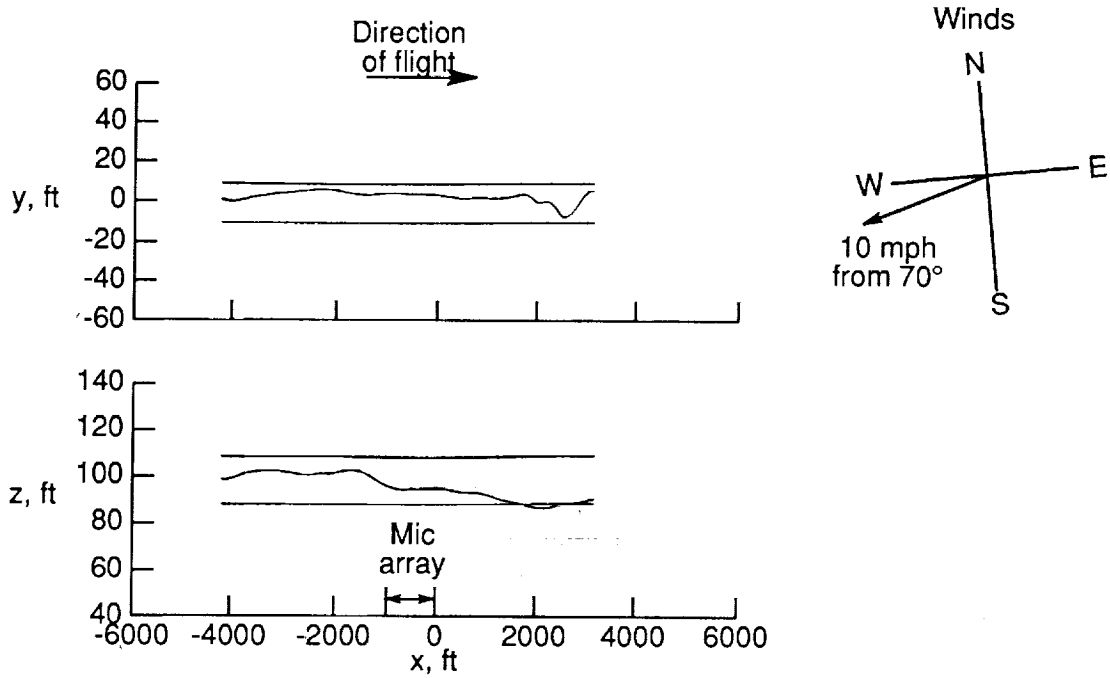


(a) $Z = 100$ ft; $\Delta Y = \Delta Z = \pm 10$ ft.

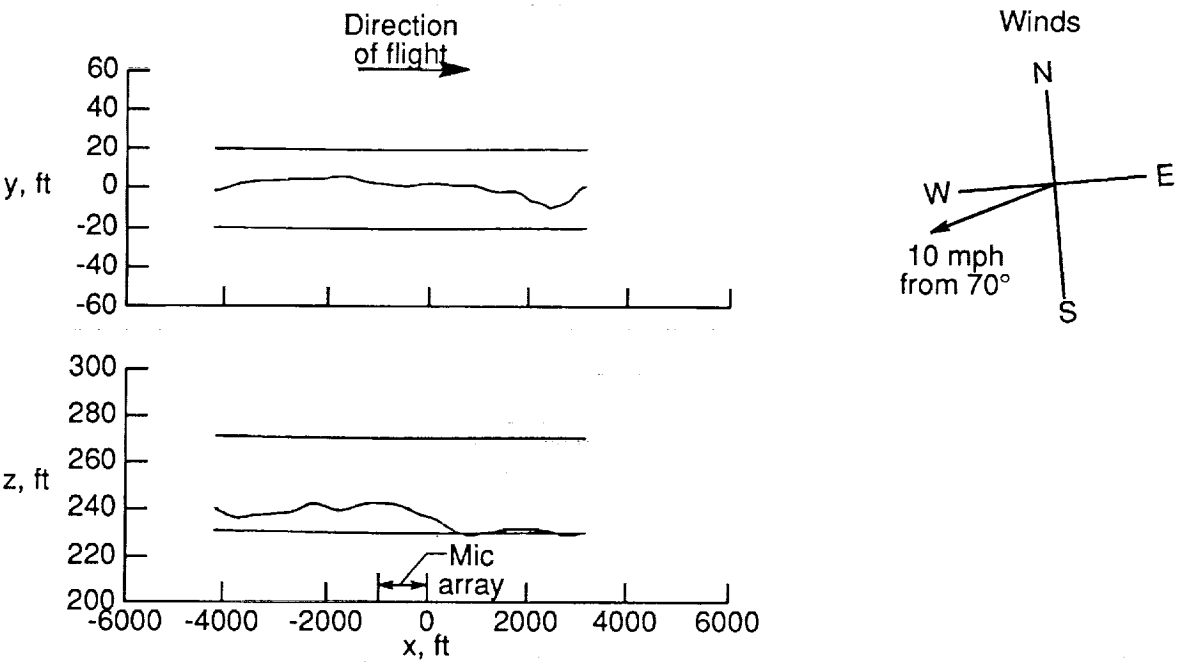


(b) $Z = 250$ ft; $\Delta Y = \Delta Z = \pm 20$ ft.

Figure 21. Effect of altitude on vertical and horizontal flight paths from 500E flight test program. Four-bladed TR; Gross weight = 3000 lb; $N_2 = 103$ percent; $V = 80$ knots.

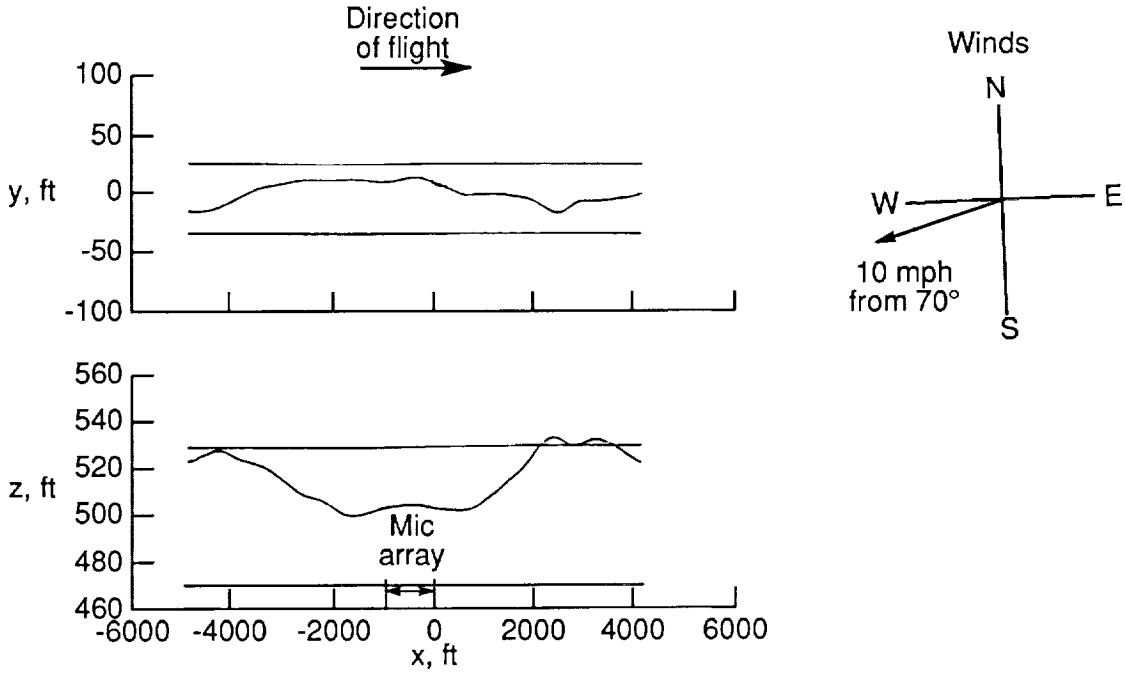


(c) $Z = 500$ ft; $\Delta Y = \Delta Z = \pm 30$ ft.

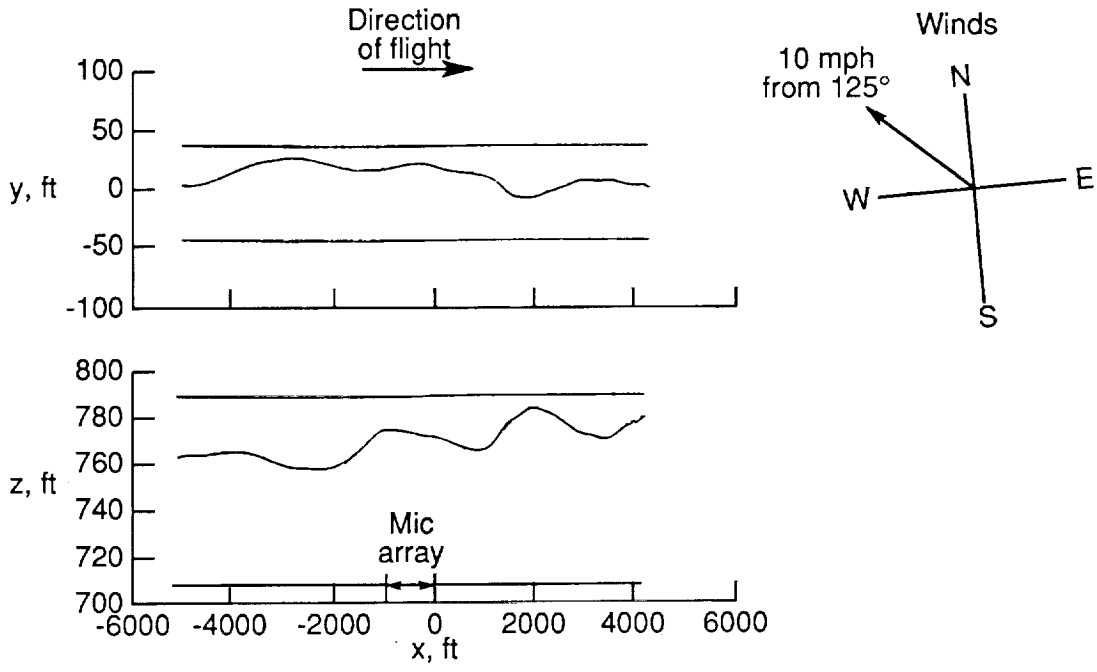


(d) $Z = 750$ ft; $\Delta Y = \Delta Z = \pm 40$ ft.

Figure 21. Concluded.

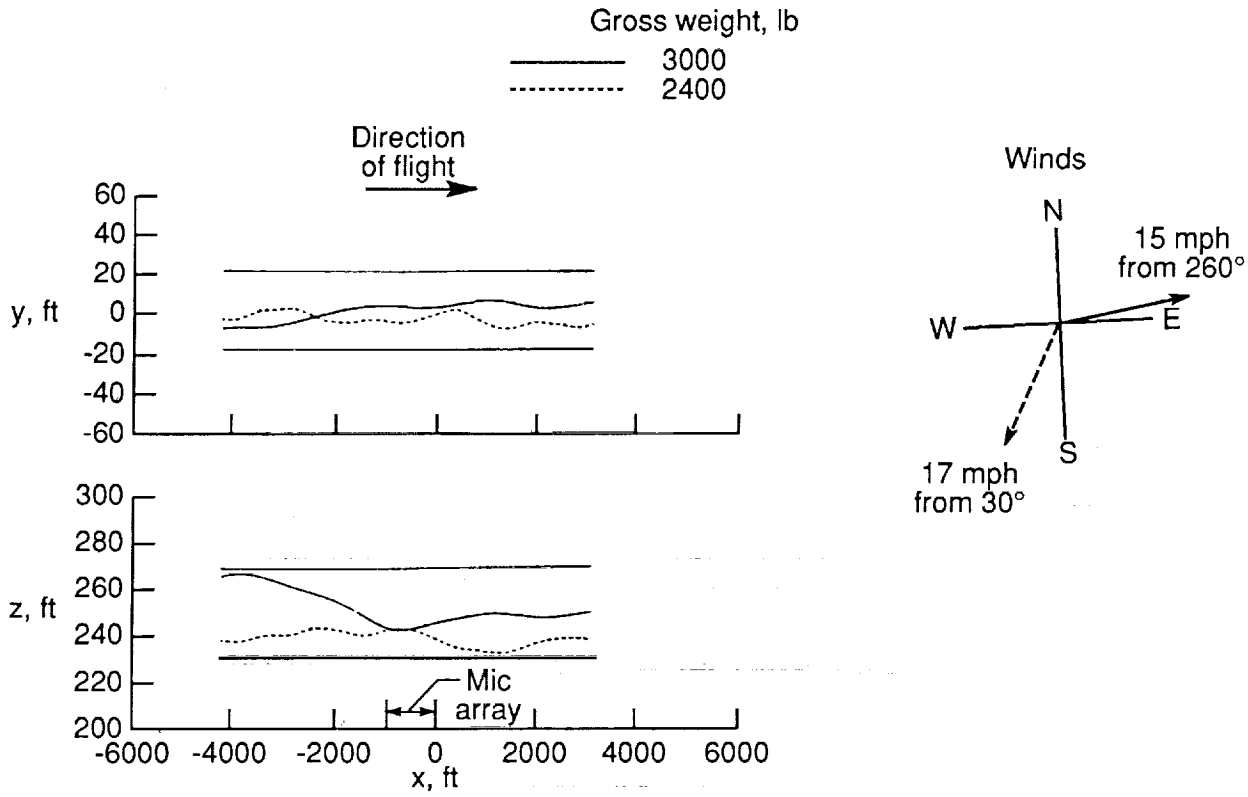


(a) $V = 80$ knots; $Z = 250$ ft; $\Delta Y = \Delta Z = \pm 20$ ft.

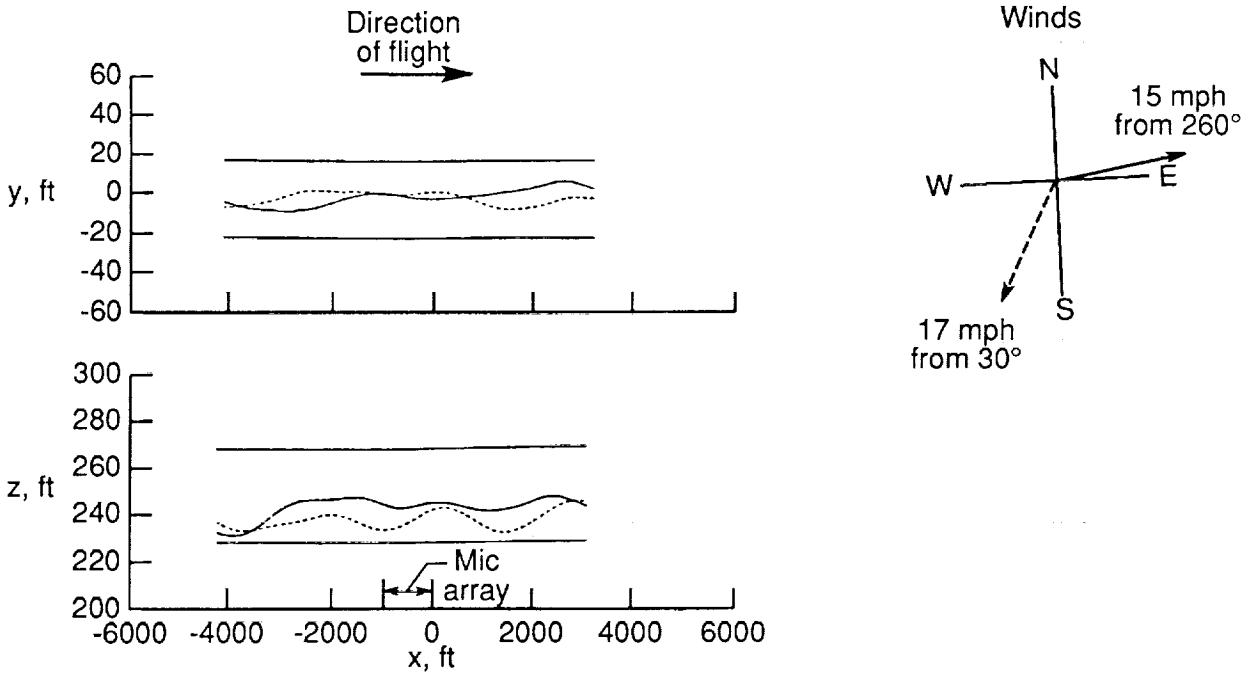


(b) $V = 120$ knots; $Z = 250$ ft; $\Delta Y = \Delta Z = \pm 20$ ft.

Figure 22. Effect of gross weight on vertical and horizontal flight paths from 500E flight test program. Two-bladed TR; $N_2 = 103$ percent.

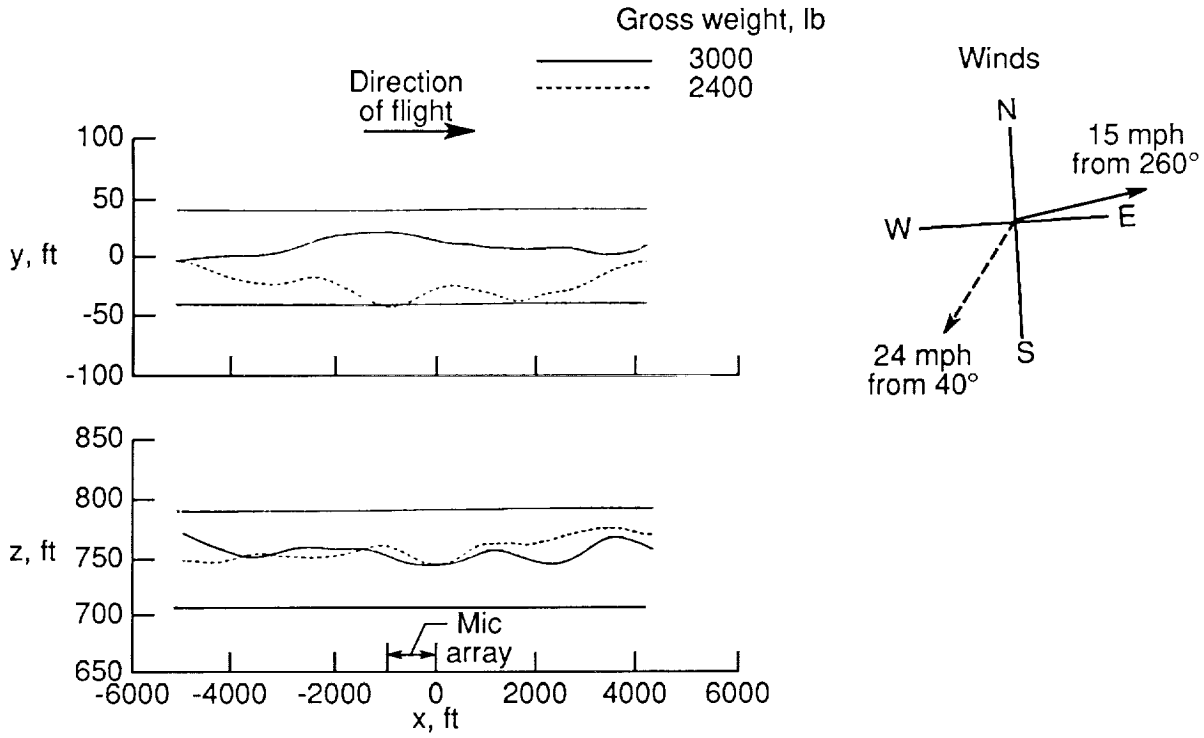


(c) $V = 80$ knots; $Z = 750$ ft; $\Delta Y = \Delta Z = \pm 40$ ft.

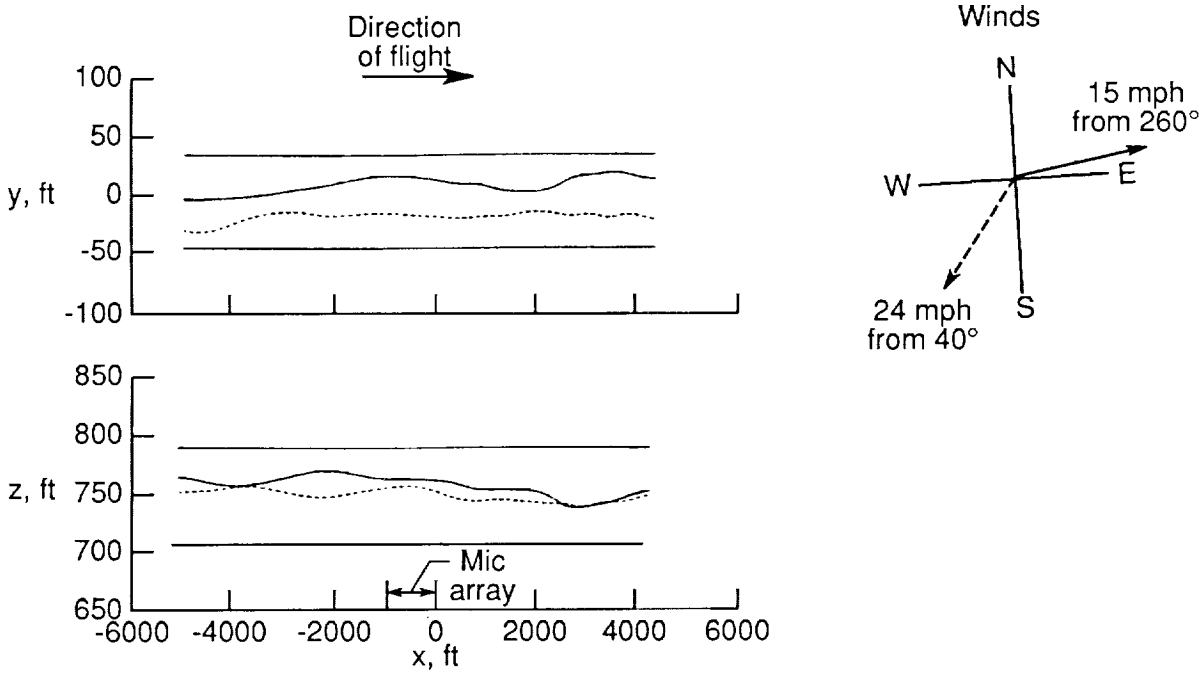


(d) $V = 120$ knots; $Z = 750$ ft; $\Delta Y = \Delta Z = \pm 40$ ft.

Figure 22. Concluded.

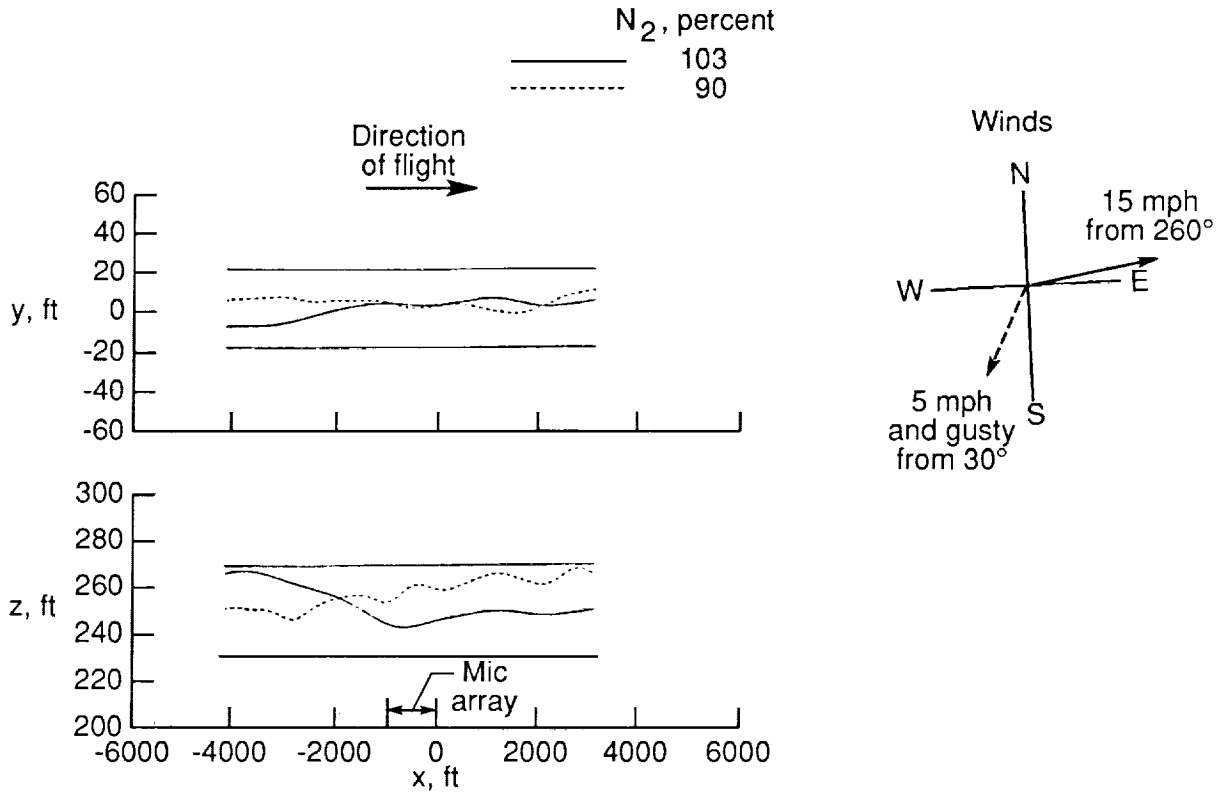


(a) $V = 80$ knots; $Z = 250$ ft; $\Delta Y = \Delta Z = \pm 20$ ft.

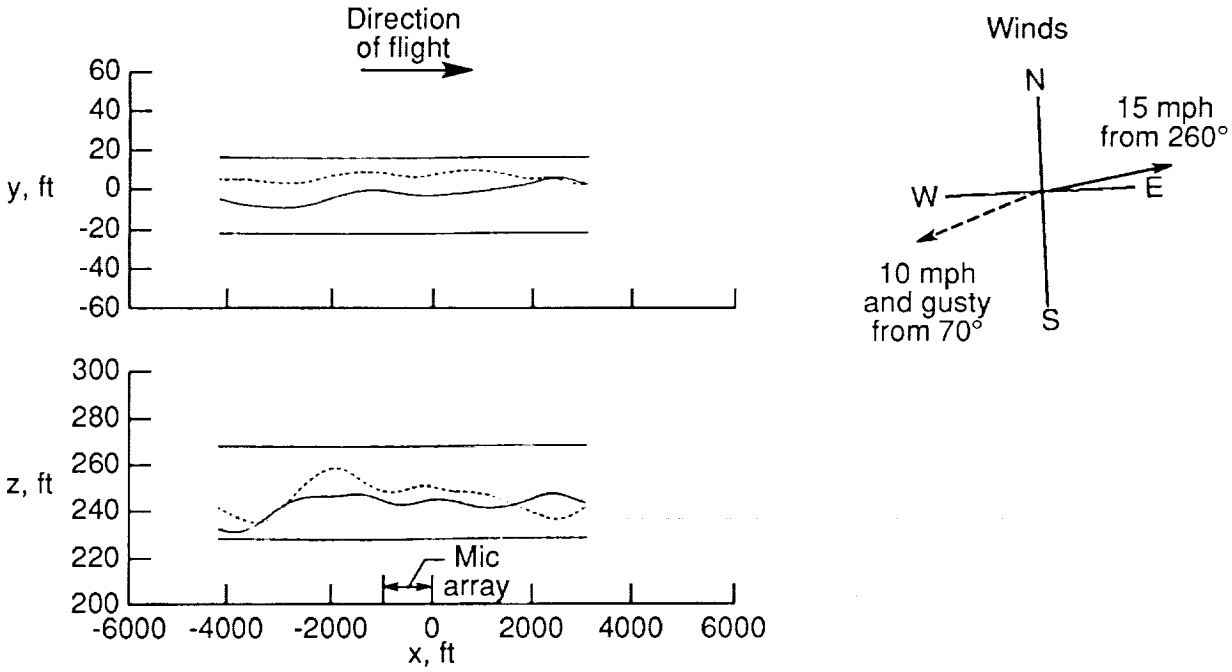


(b) $V = 120$ knots; $Z = 250$ ft; $\Delta Y = \Delta Z = \pm 20$ ft.

Figure 23. Effect of rotor speed on vertical and horizontal flight paths from 500E flight test program. Two-bladed TR; Gross weight = 3000 lb.

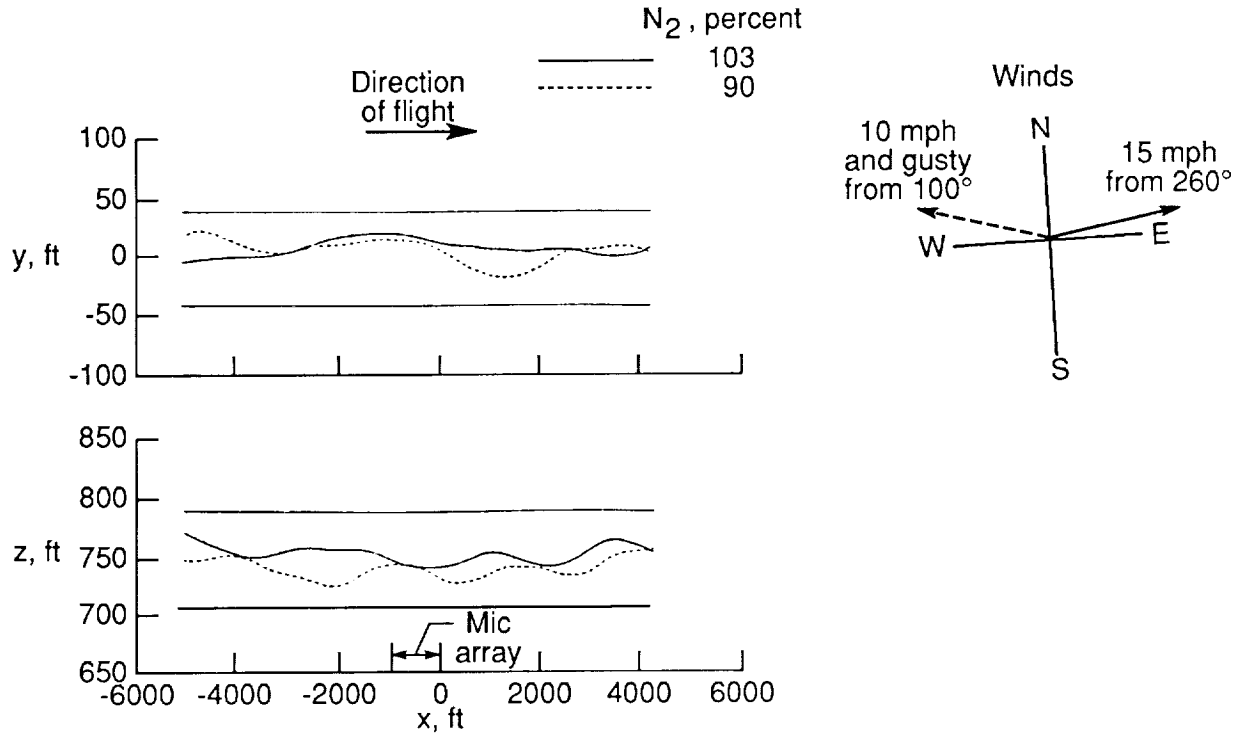


(c) $V = 80$ knots; $Z = 750$ ft; $\Delta Y = \Delta Z = \pm 40$ ft.

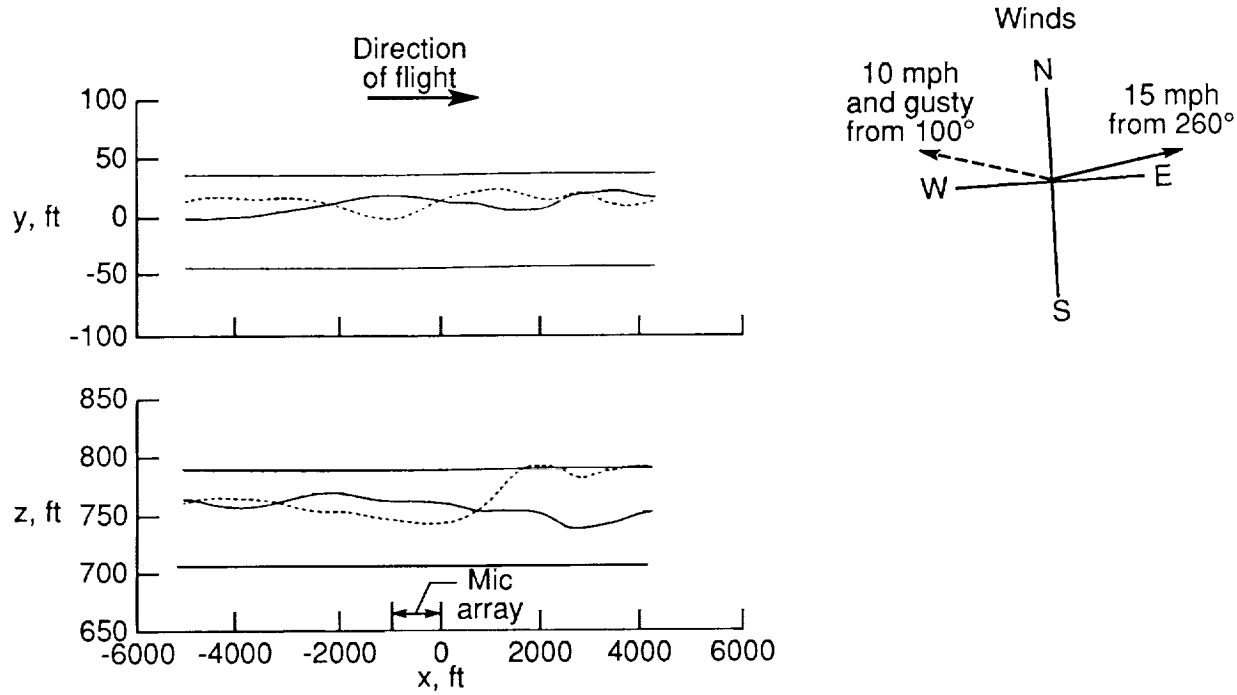


(d) $V = 120$ knots; $Z = 750$ ft; $\Delta Y = \Delta Z = \pm 40$ ft.

Figure 23. Concluded.

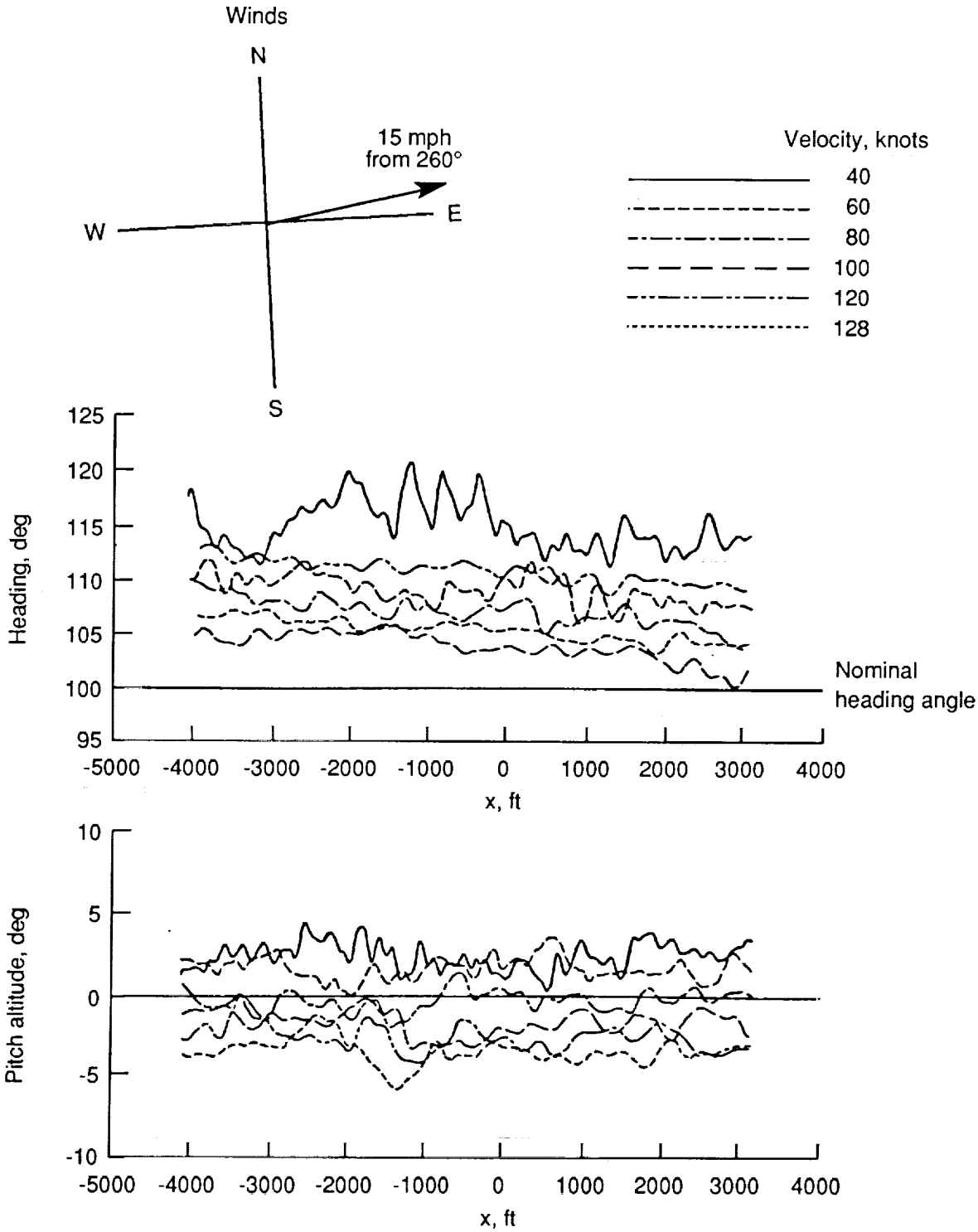


Figure 24. Effect of velocity on helicopter heading and pitch attitude from 500E flight test program. Two-bladed TR; Gross weight = 3000 lb; $N_2$ = 103 percent; $Z$ = 250 ft.

NASA
National Aeronautics and Space Administration

# Report Documentation Page

| 1. Report No. | 2. Government Accession No. | 3. Recipient's Catalog No. |
|---|---|---|
| NASA TM-4134<br>AVSCOM TR-89-B-004 | | |

| 4. Title and Subtitle | 5. Report Date |
|---|---|
| Measurement Resolution of Noise Directivity Patterns From Acoustic Flight Tests | October 1989 |
| | 6. Performing Organization Code |
| 7. Author(s)<br>David A. Conner | 8. Performing Organization Report No.<br>L-16456 |
| 9. Performing Organization Name and Address<br>Aerostructures Directorate<br>USAARTA-AVSCOM<br>Langley Research Center<br>Hampton, VA 23665-5225 | 10. Work Unit No.<br>505-63-51-07 |
| | 11. Contract or Grant No. |
| 12. Sponsoring Agency Name and Address<br>National Aeronautics and Space Administration<br>Washington, DC 20546-0001<br>and<br>U.S. Army Aviation Systems Command<br>St. Louis, MO 63120-1798 | 13. Type of Report and Period Covered<br>Technical Memorandum |
| | 14. Army Project No.<br>1L162211A47A |

15. Supplementary Notes
David A. Conner: Aerostructures Directorate, USAARTA-AVSCOM, Hampton, Virginia.

16. Abstract

A study was conducted to investigate the measurement resolution of noise directivity patterns from acoustic flight tests. Directivity-angle resolution is affected by the data reduction parameters, the aircraft velocity and flyover altitude, and deviations of the aircraft from the desired flight path. Equations are developed that determine bounds for the lateral- and longitudinal-directivity-angle resolution as a function of the nominal directivity angle. The equations are applied to a flight test data base, and the effects of several flight conditions and data reduction parameters on the directivity-angle resolution are presented. The maximum directivity-angle resolution typically occurs when the aircraft is at or near the overhead position. In general, directivity-angle resolution improves with decreasing velocity, increasing altitude, increasing sampling rate, decreasing block size, and decreasing block averages. Deviations from the desired ideal flight path will increase the resolution. For the flight experiment considered in this study, an average of two flyovers were required at each test condition to obtain an acceptable flight path. The ability of the pilot to maintain the flight path improved with decreasing altitude, decreasing velocity, and practice. Because of the prevailing wind conditions, yaw angles of as much as 20° were required to maintain the desired flight path.

| 17. Key Words (Suggested by Authors(s)) | 18. Distribution Statement |
|---|---|
| Acoustics<br>Flight testing<br>Acoustic directivity resolution<br>Aircraft flyover noise | Unclassified - Unlimited<br><br>Subject Category 71 |

| 19. Security Classif. (of this report) | 20. Security Classif. (of this page) | 21. No. of Pages | 22. Price |
|---|---|---|---|
| Unclassified | Unclassified | 41 | A03 |





For sale by the National Technical Information Service, Springfield, Virginia 22161-2171